Eur. J. Mineral.
2005, **17**, 915-932

Hagendorfite (Na,Ca)$MnFe_2(PO_4)_3$ from type locality Hagendorf (Bavaria, Germany): crystal structure determination and ^{57}Fe Mössbauer spectroscopy

GÜNTHER J. REDHAMMER[1,2]*, GEROLD TIPPELT[1], MANFRED BERNROIDER[1], WERNER LOTTERMOSER[1], GEORG AMTHAUER[1], and GEORG ROTH[2]

[1]Divison of Mineralogy and Material Science, University of Salzburg, Hellbrunnerstr. 34, A-5020 Salzburg, Austria
[2]Institute of Crystallography, University of Technology (RWTH) Aachen, Jägerstr. 17/19, D-52056 Aachen, Germany

Abstract: The crystal structure of hagendorfite (Na,Ca)$MnFe_2(PO_4)_3$ from type locality has been determined and it was found to be isostructural with alluaudite. It accepts space group symmetry *C*2/*c* both at room temperature and at 100 K. At room temperature the lattice parameters are a = 11.9721(9) Å, b = 12.5988(8) Å, c = 6.5029(5) Å, β = 114.841(8)° with Z = 4. For reasons of comparison the structure of an alluaudite *sensu strictu (s.s.)* from Buranga (Rwanda) was re-determined. The specific arrangement of M(1) and M(2) octahedral sites and of P(1) and P(2) tetrahedral sites gives rise to two different channels aligned along the crystallographic *c*-axis, containing the A(1) and A(2)' sites. In both compounds the A(1) site is fully occupied and shows a mixed occupation of Na^+, Ca^{2+} and Mn^{2+} (hagendorfite) and Ca^{2+} and Na^+ (alluaudite s.s.). The A(2)' is fully occupied by Na^+ in hagendorfite and partly filled by 0.14 Na^+ atoms per formula unit in Buranga alluaudite. The structural topology of hagendorfite is described in detail and structural parameters are compared to alluaudite *s.s.* and to other, mostly synthetic compounds also crystallizing in the alluaudite structure type. ^{57}Fe Mössbauer spectroscopy shows that iron is exclusively in the trivalent state in alluaudite *s.s.* while in hagendorfite about $^2/_3$ of the total iron are in the divalent state. The ferrous iron resonance absorption contribution appears to be broad and can only be refined with four different Fe^{2+} subcomponents, which are all ascribed to the M(2) site. The four different spectroscopic signals presumably arise from different next nearest neighbour occupations of adjacent M(2) and A(1) sites.

Key-words: structure determination, ^{57}Fe Mössbauer spectroscopy, hagendorfite, alluaudite, Na-Ca-Fe-Mn phosphates.

1. Introduction

The mineral hagendorfite (Na,Ca)$MnFe_2(PO_4)_3$ was first described by Strunz (1954) as a greenish-black sparry mineral which is similar in appearance to coarse sparry hornblende. Among other localities the mineral occurs in Hagendorf-Süd (Bavaria, Germany) at Cornelia Mine. According to the Dana classification it belongs to the group of anhydrous phosphates with $(A^+B^{2+})_5(XO_4)_3$, alluaudite subgroup (Nr. 38.2.3., Gaines *et al.*, 1997) and it was named after the type-locality Hagendorf. It occurs in the so-called Hagendorf-pegmatite as a primary phosphate (Fransolet *et al.*, 1994, 1997, 2004) together with triphylite Li(Fe,Mn)(PO_4) or wolfeite $(Fe,Mn)_2(OH/PO_4)$. It is found as greenish-black sparry masses without macroscopically visible crystals. Other minerals associated with hagendorfite are apatite and rockbridgeite $Fe^{2+}Fe^{3+}{}_4[(OH)_5/(PO_4)_3]$ (Mücke, 1981).

The crystal structure of hagendorfite itself has not been reported specifically, however, it is assumed to be isostructural with alluaudite *sensu strictu (s.s.)*. The structure of the latter was determined by Moore (1971) in the monoclinic space group *C*2/*c* on a natural specimen from Buranga-pegmatite, Rwanda. The alluaudite mineral group contains a number of anhydrous Na-Ca-Fe-Mn bearing phosphates with general formula [A(2)][A(1)]M(1)$M(2)_2(PO_4)_3$ with Z = 4 (Moore, 1971). A(1) is mainly occupied by Na^+ and Ca^{2+}, A(2) by Na^+ or vacancies, M(1) by Fe^{2+} and Mn^{2+}, M(2) by Fe^{2+}, Fe^{3+} and Mn^{2+}. Apart from these main constituents, Li^+, K^+, Mg^{2+}, Zn^{2+} and Al^{3+} are found in natural alluaudite-type compounds (Moore, 1971; Moore & Ito, 1979). Depending on chemistry and cation site distribution on M(1) and M(2), mineral species are classified into varulite, alluaudite, ferroalluaudite or hagendorfite. If M(2) is occupied mainly by trivalent iron the term alluaudite is used, whereas the name hagendorfite is used if ferrous iron dominates the M(2) site; varulite has Mn^{2+} dominating M(2) (Moore, 1971; Moore & Ito, 1979). If the Al^{3+} content reaches or exceeds one atom per formula unit, the cations Al^{3+}, Fe^{3+} and Fe^{2+} can be ordered and

*E-mail: guenther.redhammer@aon.at

DOI: 10.1127/0935-1221/2005/0017-0915
0935-1221/05/0017-0915 $ 8.10
© 2005 E. Schweizerbart'sche Verlagsbuchhandlung. D-70176 Stuttgart

Table 1. Synthetic alluaudite-type compounds, literature references and basic structural data (recalculated from given lattice parameters and fractional atomic coordinates).

Compound	Ref.	r M(1)	r M(2)	r M-sites	*a* (Å)	*b* (Å)	*c* (Å)	β (°)	Vol. (Å^3)
$NaMnFe_2(PO_4)_3$	(a), SC	0.820	0.646	2.112	12.004	12.533	6.404	114.40	877.40
$NaMnFe_2(PO_4)_3$	(b), SC	0.820	0.645	2.110	12.001	12.538	6.405	114.45	877.32
$Na_{0.5}Li_{0.5}MnFe_2(PO_4)_3$	(b), SC	0.820	0.645	2.110	11.983	12.488	6.390	114.70	868.74
$Na_{1.5}Mn_{1.5}Fe_{1.5}(PO_4)_3$	(c), RR	0.820	0.689	2.198	12.018	12.591	6.442	114.27	888.64
$Na_{1.125}Li_{0.375}Mn_{1.5}Fe_{1.5}(PO_4)_3$	(c), RR	0.820	0.689	2.198	12.013	12.543	6.427	114.57	880.73
$Na_{0.75}Li_{0.75}Mn_{1.5}Fe_{1.5}(PO_4)_3$	(c), RR	0.820	0.689	2.198	12.006	12.515	6.426	114.78	876.64
$NaMnFe_{1.5}In_{0.5}(PO_4)_3$	(d), RR	0.816	0.682	2.179	12.064	12.641	6.428	114.63	891.09
$NaMnFe_{1.0}In_{1.0}(PO_4)_3$	(d), RR	0.813	0.720	2.254	12.131	12.746	6.470	114.84	907.85
$NaMnFe_{0.5}In_{1.5}(PO_4)_3$	(d), RR	0.813	0.757	2.327	12.222	12.845	6.507	115.11	925.00
$NaMnIn_2(PO_4)_3$	(d), RR	0.813	0.795	2.402	12.282	12.948	6.552	115.21	942.70
$Na_2Mn_2Fe(PO_4)_3$	(e), RR	0.844	0.742	2.328	12.024	12.629	6.515	114.58	899.6
$Na_2(Mn_{1.5}Fe_{0.5})Fe^{3+}(PO_4)_3$	(e), RR	0.832	0.701	2.235	11.995	12.596	6.495	114.60	892.3
$Na_2(Mn_{1.0}Fe_{1.0})Fe^{3+}(PO_4)_3$	(e), RR	0.820	0.694	2.207	11.944	12.560	6.480	114.52	884.4
$Na_2(Mn_{0.5}Fe_{1.5})Fe^{3+}(PO_4)_3$	(e), RR	0.798	0.688	2.173	11.894	12.536	6.471	114.49	878.1
$Na_2Fe_2Fe^{3+}(PO_4)_3$	(e), RR	0.780	0.695	2.170	11.849	12.539	6.486	114.51	876.8
$NaCo_3(PO_4)(HPO_4)_2$	(f), SC	0.735	0.735	2.205	11.865	12.137	6.512	114.12	855.89
$NaMn_3(PO_4)(HPO_4)_2$	(g), SC	0.820	0.820	2.460	12.179	12.405	6.660	114.62	914.78
$NaCdIn_2(PO_4)_3$	(h), RR	0.950	0.790	2.530	12.528	12.959	6.576	115.34	964.92
$NaCaCdMg_2(PO_4)_3$	(i), RR	0.979	0.720	2.419	12.005	12.675	6.546	114.55	906.02
$NaFe_{3.67}(PO_4)_3$	(j), SC	0.780	0.780	2.340	11.881	12.564	6.522	115.09	881.70
$NaFe_3(PO_4)_3$	(k), SC	0.780	0.780	2.340	11.998	12.328	6.500	114.19	877.04
$NaCdIn_2(PO_4)_3$	(l), RR	0.950	0.790	2.530	12.517	12.966	6.571	115.36	963.67
$Na_{0.75}Li_{0.25}CdIn_2(PO_4)_3$	(l), RR	0.950	0.790	2.530	12.502	12.944	6.572	115.44	960.40
$Na_{0.5}Li_{0.5}CdIn_2(PO_4)_3$	(l), RR	0.950	0.790	2.530	12.479	12.917	6.571	115.55	955.61
$Na_2GaMn_2(PO_4)_3$	(m), RR	0.820	0.720	2.260	12.019	12.559	6.495	114.63	891.20
$Na_2InMn_2(PO_4)_3$	(m), RR	0.820	0.800	2.420	12.248	12.823	6.607	114.97	940.68
$Na_2GaCd_2(PO_4)_3$	(m), RR	0.950	0.620	2.190	12.188	12.799	6.547	114.75	927.48
$Na_2FeMnCd(PO_4)_3$	(m), RR	0.950	0.733	2.415	12.169	12.685	6.524	114.51	916.32
$Na_3In_2(PO_4)_3$	(n), RR	1.020	0.790	2.600	12.450	12.786	6.592	114.17	957.33
$Na_{1.79}Mg_{1.79}Fe_{1.21}(PO_4)_3$	(o), SC	0.720	0.675	2.070	11.791	12.489	6.419	113.82	864.74
$Na_4CaFe_4(PO_4)_6$	(p), SC	1.010	0.645	2.300	12.099	12.480	6.404	113.77	884.95
$Na_2FeMn_2(PO_4)_3$	(q), RR	0.820	0.733	2.285	12.049	12.624	6.507	114.56	900.22
$AgNaFeMn_2(PO_4)_3$	(q), RR	0.820	0.733	2.285	12.085	12.684	6.498	114.54	906.12
$Ag_2FeMn_2(PO_4)_3$	(r), RR	0.820	0.733	2.285	12.147	12.733	6.500	114.53	914.53
$AgNi_3(PO_4)(HPO_4)_2$	(s), SC	0.700	0.700	2.100	11.865	12.117	6.467	113.82	850.55
$AgCo_3(PO_4)(HPO_4)_2$	(t), SC	0.735	0.735	2.205	12.035	12.235	6.541	114.14	878.92
$AgMn_3(PO_4)(HPO_4)_2$	(u), SC	0.820	0.820	2.460	12.263	12.446	6.649	114.71	921.90

Abbreviations:
R M-sites = r [M(1)+2*M(2)], the unit for "r M(1)", r M(2), r [M(1)+2*M(2)] and average bond lengths, given in <> brackets is (Å), the one of OAV and TAV is (°); SC = single-crystal structure-refinement, RR = Rietveld refinement.
(a) = Moore (1971); (b) Hatert *et al.* (2000); (c) Hatert (2004); (d) Hatert *et al.* (2003); (e) Hatert *et al.* (2005); (f) Lii & Shih (1994); (g) Leroux *et al.* (1995a); (h) Antenucci *et al.* (1993); (i) Antenucci *et al.* (1995); (j) Korzenski *et al.* (1998); (k) Corbin *et al.* (1986); (l) Hatert *et al.* (2002); (m) Durio *et al.* (2002); (n) Lii & Ye (1997); (o) Hidouri *et al.* (2004a); (p) Hidouri *et al.* (2004b); (q) Daidouh *et al.* (2002); (r) Chouaibi *et al.* (2001); (s) Ben Smail & Jouini (2004); (t) Guesmi & Driss (2004); (u) Leroux *et al.* (1995b).

symmetry is lowered to $P2_1/c$. This is the case in the minerals of the wyllieite group.

The alluaudite structure-type can accommodate different cations and an increasing number of isostructural compounds have been synthesized and their crystal structures have been refined. A compilation is given in Table 1, together with basic structural data and literature references. The crystal-chemical role of Li in the alluaudite structure was investigated in detail along several binary solid solution series by Hatert and co-workers [$(Na_{1-x}Li_x)MnFe_2(PO_4)_3$, Hatert *et al*., 2000; $(Na_{1-x}Li_x)CdIn_2(PO_4)_3$, Hatert *et al*., 2002; $(Na_{1-x}Li_x)_{1.5}Mn_{1.5}Fe_{1.5}(PO_4)_3$, Hatert 2004; $Na_2(Mn_{1-x}Fe^{2+}{}_x)_2Fe^{3+}(PO_4)_3$ Hatert *et al*., 2005]. One starting point of their investigation was the composition

Table 1 (continued).

Compound	Ref.	<A(1)-O>	<A(2)-O>	<M(1)-O>	$OAV_{M(1)}$	<M(2)-O>	$OAV_{M(2)}$	<P(1)-O>	$TAV_{P(1)}$	<P(2)-O>	$TAV_{P(2)}$
$NaMnFe_2(PO_4)_3$	(a), SC	2.548	2.678	2.223	209.7	2.084	84.4	1.535	18.7	1.538	3.2
$NaMnFe_2(PO_4)_3$	(b), SC	2.543	2.748	2.202	252.8	2.038	94.7	1.539	8.8	1.538	1.6
$Na_{0.5}Li_{0.5}MnFe_2(PO_4)_3$	(b), SC	2.537	--	2.206	251.8	2.042	91.3	1.543	13.9	1.535	1.2
$Na_{1.5}Mn_{1.5}Fe_{1.5}(PO_4)_3$	(c), RR	2.553	2.744	2.204	246.7	2.046	95.3	1.543	8.0	1.541	1.9
$Na_{1.125}Li_{0.375}Mn_{1.5}Fe_{1.5}(PO_4)_3$	(c), RR	2.528	2.726	2.201	259.8	2.038	93.6	1.540	10.8	1.537	2.8
$Na_{0.75}Li_{0.75}Mn_{1.5}Fe_{1.5}(PO_4)_3$	(c), RR	2.555	2.710	2.225	241.1	2.050	76.3	1.570	27.1	1.546	4.4
$NaMnFe_{1.5}In_{0.5}(PO_4)_3$	(d), RR	2.534	2.708	2.254	239.0	2.049	72.4	1.550	32.1	1.531	3.5
$NaMnFe_{1.0}In_{1.0}(PO_4)_3$	(d), RR	2.517	2.713	2.243	254.6	2.047	73.3	1.554	35.5	1.530	5.3
$NaMnFe_{0.5}In_{1.5}(PO_4)_3$	(d), RR	2.583	2.709	2.215	197.6	2.085	96.5	1.530	97.3	1.502	11.4
$NaMnIn_2(PO_4)_3$	(d), RR	2.586	2.777	2.218	214.5	2.095	114.0	1.545	17.4	1.525	3.4
$Na_2Mn_2Fe(PO_4)_3$	(e), RR	2.555	2.679	2.244	216.8	2.098	96.3	1.505	115.5	1.556	33.0
$Na_2(Mn_{1.5}Fe_{0.5})Fe^{3+}(PO_4)_3$	(e), RR	2.589	2.682	2.186	235.1	2.061	95.4	1.581	18.6	1.564	11.0
$Na_2(Mn_{1.0}Fe_{1.0})Fe^{3+}(PO_4)_3$	(e), RR	2.593	2.692	2.182	222.3	2.066	86.5	1.543	16.4	1.548	6.1
$Na_2(Mn_{0.5}Fe_{1.5})Fe^{3+}(PO_4)_3$	(e), RR	2.560	2.688	2.196	223.8	2.047	79.1	1.552	12.2	1.543	2.4
$Na_2Fe_2Fe^{3+}(PO_4)_3$	(e), RR	2.658	2.687	2.195	195.9	2.058	69.4	1.522	28.1	1.544	5.7
$NaCo_3(PO_4)(HPO_4)_2$	(f), SC	2.599	2.664	2.228	204.8	2.121	121.4	1.555	23.3	1.525	4.8
$NaMn_3(PO_4)(HPO_4)_2$	(g), SC	2.622	2.687	2.231	179.1	2.132	146.1	1.540	10.0	1.554	1.2
$NaCdIn_2(PO_4)_3$	(h), RR	--	2.644	2.149	111.2	2.096	83.5	1.543	4.8	1.540	1.3
$NaCaCdMg_2(PO_4)_3$	(i), RR	--	2.606	2.237	106.5	2.174	92.5	1.545	5.3	1.541	1.6
$NaFe_{3.67}(PO_4)_3$	(j), SC	2.610	--	2.297	236.5	2.141	134.4	1.540	15.0	1.567	7.0
$NaFe_3(PO_4)_3$	(k), SC	2.571	2.657	2.311	242.8	2.100	67.1	1.533	24.4	1.535	5.1
$NaCdIn_2(PO_4)_3$	(l), RR	2.527	2.665	2.192	185.2	2.085	87.6	1.535	22.6	1.542	3.6
$Na_{0.75}Li_{0.25}CdIn_2(PO_4)_3$	(l), RR	--	2.681	2.175	108.3	2.129	102.8	1.542	2.7	1.540	1.7
$Na_{0.5}Li_{0.5}CdIn_2(PO_4)_3$	(l), RR	2.627	2.684	2.333	228.3	2.142	123.8	1.537	16.2	1.544	6.1
$Na_2GaMn_2(PO_4)_3$	(m), RR	2.625	2.631	2.338	237.6	2.144	119.2	1.513	13.6	1.552	12.1
$Na_2InMn_2(PO_4)_3$	(m), RR	2.567	2.813	2.336	250.7	2.156	98.7	1.562	45.9	1.529	6.8
$Na_2GaCd_2(PO_4)_3$	(m), RR	--	--	--	--	--	--	--	--	--	--
$Na_2FeMnCd(PO_4)_3$	(m), RR	--	--	--	--	--	--	--	--	--	--
$Na_3In_2(PO_4)_3$	(n), RR	--	--	--	--	--	--	--	--	--	--
$Na_{1.79}Mg_{1.79}Fe_{1.21}(PO_4)_3$	(o), SC	2.440	2.692	2.286	303.8	2.148	99.9	1.542	--	1.551	75.8
$Na_4CaFe_4(PO_4)_6$	(p), SC	2.634	2.682	2.448	288.7	2.151	110.7	1.545	7.6	1.539	20.0
$Na_2FeMn_2(PO_4)_3$	(q), RR	2.535	2.687	2.140	192.3	2.044	90.6	1.547	10.9	1.546	4.3
$AgNaFeMn_2(PO_4)_3$	(q), RR	2.550	2.698	2.323	307.4	2.031	71.4	1.538	5.5	1.538	2.8
$Ag_2FeMn_2(PO_4)_3$	(r), RR	2.537	2.697	2.248	232.8	2.117	71.7	1.496	64.2	1.539	5.7
$AgNi_3(PO_4)(HPO_4)_2$	(s), SC	2.597	2.708	2.278	223.9	2.093	87.7	1.573	25.6	1.509	0.8
$AgCo_3(PO_4)(HPO_4)_2$	(t), SC	2.599	2.741	2.243	243.9	2.093	83.4	1.539	19.4	1.542	0.5
$AgMn_3(PO_4)(HPO_4)_2$	(u), SC	--	2.683	2.123	115.6	2.073	84.7	1.553	4.3	1.546	0.6

$NaMnFe_2(PO_4)_3$, which corresponds to the idealized composition of the Buranga-pegmatite alluaudite (Moore, 1971).

^{57}Fe Mössbauer spectroscopy was also applied to synthetic alluaudite-type compounds mainly to characterize the valence state and distribution of iron (Korzenski *et al*., 1998; Hermann *et al*., 2002; Hatert *et al*., 2003, 2004). It was found that iron mainly occurs on the M(2) site but shows a distribution of quadrupole splitting. This occurs for both, Fe^{2+} and Fe^{3+} and was interpreted to be due to different occupation of neighbouring M(2) sites by (Na, Ca) in $Na_4CaFe_4(PO_4)_6$ (Hidouri *et al*., 2004b) or by Fe^{2+} and Fe^{3+} in $(Na_{1-x}Li_x)MnFe_2(PO_4)_3$ compounds (Hermann *et al*. 2002; Hatert *et al*., 2003, respectively). Hatert *et al*. (2005) also inserted Fe^{2+} on the M(1) site in the synthetic $Na_2(Mn_{1-x}Fe^{2+}_x)_2Fe^{3+}(PO_4)_3$ alluaudite-type solid solution series. Except Hatert *et al*. (2005) most of the samples investigated so far exhibit Fe^{3+} only or contained ferrous iron in very minor amounts.

In the present study, we present the first determination of the crystal structure of hagendorfite from type locality, including new chemical analyses and first ^{57}Fe Mössbauer data. Furthermore, we present a re-determination of the structure of alluaudite from Buranga, Rwanda. Comparison will be made between the two structures and with other synthetic alluaudite-type compounds described in literature so far. This paper, therefore, also intends to give basic crystal chemical relations and to contribute to a better crystal chemical knowledge of alluaudite-type compounds. It may be noted here that during review process the authors

Table 2. Chemical composition (wt.%) of hagendorfite from Hagendorf-Süd, Cornelia Mine, level 76, as compared to the data of Strunz (1954) and to alluaudite *s.s.* from Buranga-pegmatite, Rwanda (Fisher, 1955).

specimen	this study hag	Strunz (1954) hag	this study allu	Fisher (1955) allu
Na_2O	9.99(11)	8.47	4.85(24)	3.90
CaO	1.46(7)	1.68	4.59(26)	1.40
K_2O	--	0.17	--	--
Li_2O	--	--	n.d.	0.09
FeO	18.23(14)	15.44	--	--
Fe_2O_3	8.97(14)	13.30	28.67(29)	31.48
MnO	17.94(11)	18.50	15.04(14)	15.34
MgO	0.35(5)	0.66	0.58(15)	0.47
Al_2O_3	--	--	2.20(31)	--
P_2O_5	42.20(18)	42.26	43.84(36)	42.15
H_2O^+	--	--	--	3.55
Sum	99.15	100.48	99.78	99.84

Abbrev.: hag = hagendorfite, allu = alluaudite, n.d. = not determined

FeO and Fe_2O_3 recalculated on basis of ^{57}Fe Mössbauer spectroscopy.

became aware of the work of Hatert (2002) dealing with the crystal chemistry of synthetic and natural alluaudite-type minerals/compounds.

2. Experimental

The chemical compositions of both, the Hagendorf (hagendorfite) and the Buranga (alluaudite) samples, were determined by electron microprobe analysis. Small pieces of the sample material were embedded in epoxy - resin, polished, covered with carbon and analysed with a JEOL JXA 8600 electron microprobe (acceleration voltage 15 kV, initial beam current 40 nA, beam focused to 5 μm). NaCl, Al_2O_3, MgO, wollastonite (Ca), FeO, MnO and a natural apatite (P) were used as standards. Results of chemical analysis are given in Table 2.

For the hagendorfite sample, single-crystal X-ray diffraction intensity data were collected on a Stoe IPDS II imaging-plate diffractometer system using the rotation method (Mo*K*α radiation, pyrolytic graphite monochromator). The system is equipped with a cryo-stream liquid N_2 – cryostat (85 K ... 300 K, accuracy at least 1 K). Intensity data were collected on a greenish-black, prismatic fragment of the title compound ($0.14 \times 0.10 \times 0.09$ mm) up to 65.0° in 2θ within an ω-range of 0-180° and two different φ positions (15° and 110°); the ω rotation during imaging was 1.5°/frame. Data collection for the alluaudite sample was performed on a Bruker SMART APEX CCD-diffractometer. Intensity data were collected on a reddish-brown platy fragment ($0.18 \times 0.15 \times 0.06$ mm) in 2400 frames with increasing ω (width of 0.3° in ω at 4 different ϕ positions) and in 900 frames with increasing ϕ (width of 0.3° in ϕ). Details on data collection and experimental setup are compiled in Table 3. In both cases lattice parameters were determined from single-crystal X-ray diffraction data. Absorption correction was done empirically *via* equivalents using the SHAPE - software (Stoe & Cie, 1996). Structure solution (using Patterson methods) and subsequent refinement was carried out with the programs SHELXS-97 and SHELXL-97 (Sheldrick, 1997) as implemented in the program suite WinGX 1.64 (Farrugia, 1999). X-ray scattering factors in their ionic form, together with anomalous dispersion coefficients were taken from the International Tables for Crystallography (Wilson, 1992). The program DIAMOND 2.0 (Pennington, 1999) was used to prepare the graphical visualization of the crystal structure.

Table 3. Crystallographic data and experimental details for hagendorfite (298 K and 100 K) and alluaudite *s.s.* (298 K).

	Hagendorfite	Hagendorfite	Alluaudite s.s.
T (K)	298(2)	100(2)	298(2)
space group	*C*2/*c*	*C*2/*c*	*C*2/*c*
a (Å)	11.9721(9)	11.9492(9)	11.9941(7)
b(Å)	12.5988(8)	12.5548(8)	12.5256(7)
c (Å)	6.5029(5)	6.4966(5)	6.3973(4)
β (°)	114.841 (8)	114.816(8)	114.257(8)
V (Å3)	890.11 (11)	884.62(11)	876.23(9)
Z	4	4	4
D_x (Mg m^{-3})	3.746	3.638	3.719
Radiation type	Mo *K*α	Mo *K*α	Mo *K*α
θ range (°)	2.5 - 32.2	2.5 - 29.1	2.5 - 28.7
μ (mm^{-1})	5.45	5.45	5.52
Crystal form	Prism	Prism	Flake
Crystal colour	dark green	dark green	brown
Crystal size (mm)	0.14	0.14	0.18
	0.10	0.10	0.15
	0.09	0.09	0.06
Absorption correction	Numerical	Numerical	Numerical
T_{min}	0.525	0.521	0.35
T_{max}	0.604	0.609	0.53
No. of measured,	6982,	6871,	5798,
Independent and	1196,	1177,	1089,
Observed reflections	1028	1037	1074
Criterion for observed	$I > 2\sigma(I)$	$I > 2\sigma(I)$	$I > 2\sigma(I)$
R_{int}	0.065	0.064	0.037
θ_{max} (°)	29.1	29.1	28.7
Range of *h,*	–16 → 16	–16 → 16	–15 → 15
k,	–17 → 17	–17 → 17	–16 → 16
l	–8 → 8	–8 → 8	–8 → 8
$R[F^2 > 2\sigma(F^2)]$,	0.028,	0.027,	0.019,
$wR(F^2)$,	0.066,	0.062	0.048,
S	1.01	1.052	1.08
No. of reflections	1196	1177	1089
No. of parameters	100	100	99
Weighting scheme (a/b)	0.036	0.032/ 0.58	0.026/ 1.104
$(\Delta/\sigma)_{max}$	0.001	0.001	0.001
$\Delta\rho_{max}$, $\Delta\rho_{min}$ (e Å^{-3})	0.56, -1.02	0.62, -1.17	0.41, -0.39
Extinction method	SHELXL	SHELXL	SHELXL
Extinction coefficient	0.0030 (4)	0.0028(3)	0.0000(2)

$w = 1/[s^2(Fo^2) + (aP)^2+(bP)]$ where $P = (Fo^2 + 2Fc^2)/3$

Transmission ^{57}Fe Mössbauer spectra between 80 K and 300 K were collected using a Mössbauer apparatus in hori-

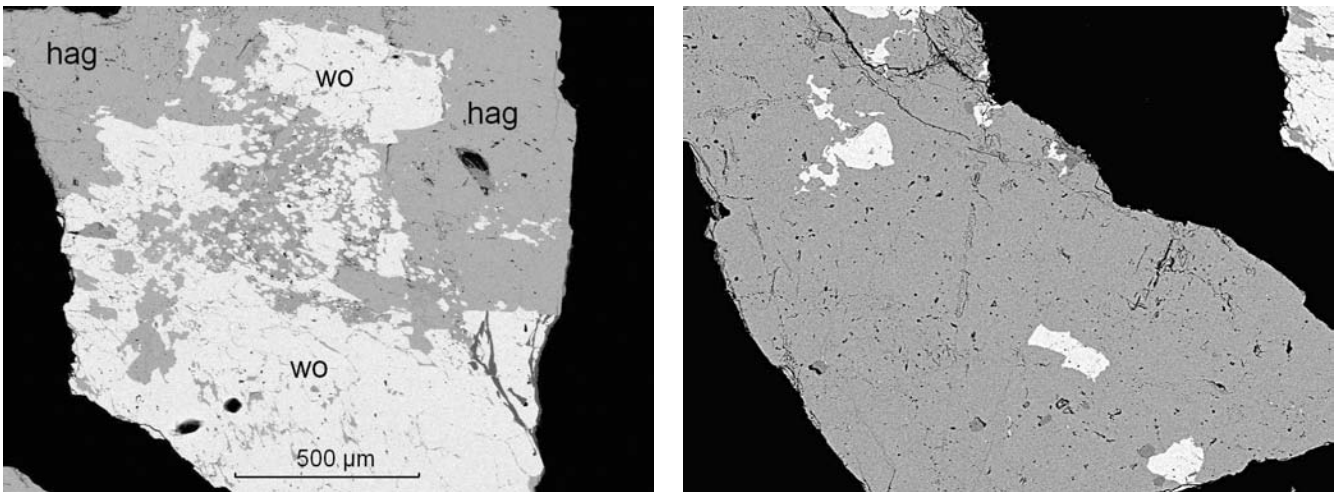

Fig. 1. Backscattered electron images of hagendorfite grains (hag = dark gray phase) with intergrowth of wolfeite (wo = light gray phase).

zontal arrangement (^{57}Co/Rh single line thin source, constant acceleration, symmetric triangular velocity shape, multi-channel analyser with 1024 channels, and velocity calibration to α-Fe). For Mössbauer absorber preparation, samples were carefully ground under ethanol (to avoid oxidation), mixed with epoxy resin and filled into Cu – rings (inner diameter 10 mm), covered with a high purity Al – foil on one side. The folded spectra were analyzed using both the classical Hamiltonian site analysis (Lorentzian shaped doublets) and the Voigt-based quadrupole splitting distribution (QSD) method (Rancourt & Ping, 1991), as implemented in the program suite RECOIL. Complete thickness correction was applied to all Mössbauer spectra before analysis (Rancourt *et al*., 1993).

3. Results and discussion

3.1. Sample material and mineral chemistry

Two natural samples were used for the present study. The hagendorfite sample used is from locality Hagendorf-Süd, level 76 and was obtained from the Mineralogical State Collection, Munich, Museum Kingdom of Crystals, sample number MSM#2914, courtesy Dr. R. Hochleitner. The sample was a massive black-greenish piece, approximately 3 × 2 × 2 cm^3 in size, consisting of massive sparry hagendorfite associated with minor amounts of wolfeite. Several small pieces were split off the main part, three of them were used for electron microprobe analysis, and the other ones were crushed further to a grain size below about 200 µm. A single phase batch was obtained by hand-picking. This material was then used for both, the Mössbauer absorber preparation as well as single crystals for X-ray diffraction.

Electron microprobe analysis (EMPA) was performed on three different grains, approximately 2 mm in diameter. It was found that hagendorfite occurs together with wolfeite (Fig. 1). The hagendorfite crystals themselves are remarkably homogeneous in terms of chemical composition and do not show any significant variations within each grain. The results of the chemical analyses are compiled in Table 2, together with the results obtained by Strunz (1954).

Our recent chemical analysis on hagendorfite is in quite good agreement with the one of Strunz (1954), except for the Fe^{2+}/Fe^{3+} ratio, which is more accurate in the present study as it is based on detailed ^{57}Fe Mössbauer analysis which gives much more precise Fe^{2+}/Fe^{3+} ratios. Combining the data, obtained by EMPA, with the data from ^{57}Fe Mössbauer analysis, the structural formula of the hagendorfite sample has to be written as:

$$\{Na_{1.64}Ca_{0.13}Mn_{0.20}\}(Mn_{1.00})[Fe^{2+}_{1.29}Fe^{3+}_{0.57}Mg_{0.04}Mn_{0.09}]P_{3.03}O_{12}$$

with { } representing the A sites, ( ) the M(1) and [ ] the M(2) sites. As Fe^{2+} dominates M(2) and Mn^{2+} dominates the M(1) site the specimen indeed has to be named hagendorfite. The composition of wolfeite, associated with hagendorfite is given as $(Mn_{0.77}Fe^{2+}_{1.22})(OH/P_{1.00}O_4)$.

The alluaudite sample studied here is from the Buranga-pegmatite, Rwanda and was obtained from the Museum of Natural History, Vienna; sample number L8155, courtesy Dr. V. Hammer. The sample obtained was a 1.5 × 1 × 1 cm^3 large piece of reddish-brown sparry masses of alluaudite, associated with phosphosiderite, strengite and bermanite. Part of the sample was prepared for microprobe analysis; the rest was crushed, hand-picked and used for ^{57}Fe Mössbauer spectroscopy and single-crystal X-ray diffraction. The results of the EMPA analysis are included in Table 2, together with a wet chemical analysis by Fisher (1955), also on Buranga-pegmatite alluaudite. In contrast to the findings of Fisher (1955) we found distinctly higher Na_2O and CaO contents, minor amounts of MgO and Al_2O_3 but similar MnO and Fe_2O_3 contents. We have no indication that our Buranga alluaudite sample contains significant amounts of water as stated by Fisher (1955). Furthermore, the composition found is in reasonable agreement with the one derived from the structure refinement which was done prior to the chemical analysis. From Mössbauer spectroscopy, there are no signs for ferrous iron in the alluau-

Table 4. Fractional atomic coordinates for hagendorfite (298 K and 100 K) and alluaudite (298 K).

	x	y	z	U(eq)
Hagendorfite, T = 100 K				
A(1)	1/2	0.0	0.0	0.0481(5)
A(2)'	0.0	-0.0192(2)	1/4	0.0241(7)
M(1)	0.0	0.2672(1)	1/4	0.0104(2)
M(2)	0.2790(1)	0.6580(1)	0.3650(1)	0.0094(2)
P(1)	0.0	-0.2885(1)	1/4	0.0103(2)
P(2)	0.2344(1)	-0.1080(1)	0.1273(1)	0.0109(2)
O(1)	0.4557(2)	0.7180(2)	0.5371(3)	0.0122(4)
O(2)	0.986(2)	0.6353(2)	0.2419(4)	0.0192(5)
O(3)	0.3361(2)	0.6647(1)	0.1028(3)	0.0150(4)
O(4)	0.1282(2)	0.4035(2)	0.3199(4)	0.0170(4)
O(5)	0.2233(2)	0.8238(2)	0.3143(3)	0.0152(4)
O(6)	0.3284(2)	0.5001(2)	0.3856(4)	0.0162(4)
Hagendorfite, T = 298 K				
A(1)	1/2	0.0	0.0	0.0520(6)
A(2)'	0.0	-0.0192(2)	1/4	0.0359(9)
Mn(1)	0.0	0.2670(1)	1/4	0.0149(2)
Fe(2)	0.2788(1)	0.6577(1)	0.3645(1)	0.0125(2)
P(1)	0.0	-0.2881(1)	1/4	0.0128(2)
P(2)	0.2348(1)	-0.1080(1)	0.1276(1)	0.0133(2)
O(1)	0.4555(2)	0.7180(2)	0.5376(3)	0.0159(4)
O(2)	0.0983(2)	0.6360(2)	0.2409(4)	0.0225(5)
O(3)	0.3357(2)	0.6640(2)	0.1025(3)	0.0182(4)
O(4)	0.1284(2)	0.4033(2)	0.3201(4)	0.0209(5)
O(5)	0.2237(2)	0.8242(2)	0.3143(3)	0.0194(4)
O(6)	0.3273(2)	0.5000(2)	0.3848(4)	0.0209(5)
Alluaudite s.s., T = 298 K				
A(1)	1/2	0.0	0.0	0.0371(3)
A(2)'	0.0	-0.0136(8)	1/4	0.0387(3)
M(1)	0.0	0.2598(1)	1/4	0.0122(2)
M(2)	0.2813(1)	0.6521(1)	0.3721(1)	0.0093(1)
P(1)	0.0	-0.2852(1)	1/4	0.0096(1)
P(2)	0.2428(1)	-0.1086(1)	0.1319(1)	0.0097(1)
O(1)	0.4531(1)	0.7150(1)	0.5330(2)	0.0125(3)
O(2)	0.0993(1)	0.6397(1)	0.2412(2)	0.0163(3)
O(3)	0.3275(1)	0.6640(1)	0.1024(2)	0.0133(3)
O(4)	0.1211(1)	0.3980(1)	0.3131(2)	0.0163(3)
O(5)	0.2259(1)	0.8221(1)	0.3185(2)	0.0134(3)
O(6)	0.3105(1)	0.5023(1)	0.3745(2)	0.0170(3)

U_{eq} is the equivalent isotropic atomic displacement parameter (Å²). Numbers in brackets are the estimated standard deviations and refer to the last digit.

dite sample, *i.e.* iron is solely in the trivalent state. The structural formula of the Buranga-pegmatite alluaudite may be therefore written as:
$\{Na_{0.76}Ca_{0.40}\}(Mn_{1.00})[Fe^{3+}_{1.73}Al_{0.21}Mg_{0.04}Mn_{0.04}]P_{3.00}O_{12}$.

3.2 Single crystal X-ray diffraction

The analysis of systematic absences indicated the space group *C*2/*c* for both compounds at all temperatures investigated. Structure solution on the hagendorfite 298 K data using Patterson methods and subsequent full-matrix structure refinement on F^2 using anisotropic displacement parameters yielded a structure model with six different oxygen atom positions, two sites for phosphorus, two sites for (Fe,Mn) and two sites for Na^+ and Ca^{2+}. As the structure of the title compound was found to be isostructural with alluaudite, fractional atomic coordinates were transformed such that they are comparable to the ones originally given by Moore (1971), a nomenclature that is also used in the more recent literature (*e.g.* Hatert *et al.*, 2000; Hatert 2004). As iron and manganese cannot be distinguished by conventional X-ray diffraction analysis, it was assumed, that Mn^{2+} occupies the M(1) site, Fe^{3+} was located onto the M(2) site. For both sites the occupation factor was allowed to vary freely during refinement. It was found that they converge to values expected for fully occupied sites, thus no vacancies are assumed to occur on M(1) and M(2) sites in hagendorfite. In the final refinement, occupations for M(1) and M(2) were fixed to their ideal values. The A(2)′ site (0, y, 1/4) with y ≈ 0 is occupied by Na exclusively, whereas on the A(1) site, there is a distribution of Na, Ca^{2+} and Mn. Attempts to assign Ca^{2+} and/or Mn^{2+} to the A(2)′ site failed. The amount of Ca^{2+}, found by structure refinement of X-ray diffraction data was 0.17 atoms per formula unit (apfu) in close agreement with the EMP analysis. Site occupations for the 100 K data of hagendorfite are identical to the ones at 298 K within experimental error which further corroborates the model.

The fractional coordinates found for hagendorfite were used as an initial model for the refinement of the alluaudite data. However, the A(2)′ position was removed. According to Moore (1971) this position is vacant in Buranga alluaudite. For the A(1) site, a full occupation was assumed and a distribution of Na^+ and Ca^{2+} allowed. This yielded an occupation of 0.68 Na^+ + 0.32 Ca^{2+}, giving a total Ca^{2+} content, which is very close to the value determined by EMP analysis (0.35 apfu Ca^{2+}). With this model, however, distinct residual electron density remained at (0, -0.015, 0.25) which exactly corresponds to the A(2)′ position. Thus this position was introduced into the refinement, allowing the occupation of Na^+ to vary freely giving a final occupation for A(2)′ of 0.16 Na^+ + 0.84 vacancies. Na^+ was chosen as the chemical analysis yielded higher Na content as the one found by structure refinement. Accordingly the A(2)′ position in Buranga alluaudite is not completely vacant as stated by Moore (1971) but filled with 0.16 Na^+ apfu. Furthermore, the occupation of the M(1) and M(2) sites were also allowed to vary. While for the M(1) site a full occupation was obtained, the M(2) site showed some deficits when filled with Fe^{3+} only. Introducing Al^{3+} to the refinement yielded 0.26 Al^{3+} (+ Mg^{2+}) in close agreement with the Al^{3+} + Mg^{2+} content found later on by EMPA.

Table 3 contains a summary of experimental conditions during data collection and the structure refinement parameters. Table 4 gives refined fractional atomic coordinates and isotropic displacement parameters, whereas the anisotropic displacement parameters are given in the Crystallographic Information File CIF[1]. Table 5 compiles selected bond lengths, bond angles and distortion parameters.

[1]The CIF is available upon request from the first author or through the EJM Editorial Office - Paris

3.2.1. Lattice parameters

The lattice parameters of hagendorfite (Table 3) are significantly different from those of alluaudite *s.s.*, reflecting the differences in chemical composition. The *a* parameter is smaller, whereas *b* and especially *c* are distinctly larger as compared to Buranga-alluaudite. Our data for the Buranga-alluaudite, however, compare well with literature. They are only slightly smaller than the ones given by Hatert *et al*., (2000) for the idealized synthetic compound $NaMnFe_2(PO_4)_3$. Further, our data are slightly smaller than the lattice parameters for the Buranga alluaudite, recalculated by Hatert *et al*., (2000) from the X-ray powder diagram of Fisher (1955). This offset is most probably due to different experimental setups. Figure 2 depicts lattice parameters of several different alluaudite-type compounds, taken from literature, *vs.* the average of the ionic radius of the M-site cations, calculated as $<r>_{M\text{-}site} = <r>_{M(1)} + 2* <r>_{M(2)}$. Although there is scatter among the data points, there is a positive correlation between lattice parameters and the nominal size of the M-site cations. However, the scattering, which is most pronounced for *b*, suggests that the A-site cations also have an influence on the size of lattice parameters. It has been noted by Hatert *et al*. (2000, 2002) and Hatert (2004) that an almost linear decrease of *a*, *b*, and *c* with increasing Li^+ - content is observed for the $(Na_{1-x}Li_x)$ substitution in alluaudite-type compounds. In this series, the *b* axis shows the most pronounced changes. This is primarily due to the shortening of the A(1)-O(2) and A(1)-O(4) bonds, which form a square parallel to the *b* axis (Hatert, 2004) thus influencing the *b*-direction most. Thus the scatter in Fig. 2b can be ascribed to the influence of the A-site cations. As can be seen from Fig. 2c, the *c* lattice parameter shows the smoothest trend with average M-site cationic radius, suggesting that *c* is quite insensitive to changes in the A-site occupation but mainly depends on the size of the M-cations. The distinct differences of the *c* lattice parameters between hagendorfite and alluaudite can thus be explained by the difference in average M(2) site cationic radii, which are – based on chemistry and ionic radii given by Shannon & Prewitt (1969) – 0.740 Å and 0.648 Å respectively (Table 1). The average A(1) cationic radius is smaller in hagendorfite (1.107 Å) as compared to 1.146 Å in alluaudite. So in principle, the *a* and especially the *b* lattice parameter in hagendorfite should be expected to be smaller as compared to alluaudite. However, it has to be taken into account that the A(2)′ site is completely filled in hagendorfite but almost empty in alluaudite. Comparing the lattice parameters of $NaMnFe_2(PO_4)_3$ (Hatert *et al*., 2000) with only small amounts of sodium occupying the A(2)′ site and a completely filled A(1) site, with the compound $Na_2Mn_2Fe(PO_4)_3$ (Daidouh *et al*., 2002) with both sites completely filled with sodium, it is evident that all lattice parameters are larger in the latter compound (also see Table 1). A similar observation was made by Korzenski *et al*. (1998) when comparing $NaFe_{3.67}(PO_4)_3$ with 0.67 apfu Fe on the A(1) site and a completely filled A(2)′ site with $NaFe_3(PO_4)_3$ with sodium at the A(2)′ site only. Again, the former compound shows a larger unit cell (Table 1). Taking

Table 5. Selected bond lengths (Å), bond angles (°) and distortion parameters for hagendorfite and alluaudite.

	hagendorfite	hagendorfite	alluaudite s.s.
T (K)	100(1)	298(1)	298(1)
A(1)-O2 x2	2.278(2)	2.286(2)	2.313(1)
A(1)-O4 x2	2.337(2)	2.343(2)	2.316(1)
A(1)-O4 x2	2.586(2)	2.593(2)	2.568(1)
A(1)-O2 x2	2.957(2)	2.970(2)	2.974(1)
<A(1)-O>	2.539	2.548	2.543
A(2)'-O6 x2	2.407(2)	2.418(2)	2.544(2)
A(2)'-O6 x2	2.561(2)	2.574(2)	2.706(2)
A(2)'-O1 x2	2.794(2)	2.801(2)	2.823(1)
A(2)'-O3 x2	2.917(2)	2.920(2)	2.918(1)
<A(2)'-O>	2.670	2.678	2.748
M(1)-O3 x2	2.198(2)	2.211(2)	2.238(1)
M(1)-O4 x2	2.213(2)	2.221(2)	2.189(1)
M(1)-O1 x2	2.229(2)	2.236(2)	2.179(1)
<M(1)-O>	2.214	2.223	2.202
$Vol_{M(1)}$	13.16	13.33	12.71
$BLD_{M(1)}$	0.46	0.40	1.09
$ELD_{M(1)}$	8.79	8.77	9.87
$OAV_{M(1)}$	210.17	209.68	252.77
$(e_u/e_s)_{M(1)}$	1.21	1.21	1.25
M(2)-O2	1.983(2)	1.983(2)	1.996(1)
M(2)-O6	2.056(2)	2.059(2)	1.908(1)
M(2)-O1	2.072(2)	2.078(2)	2.046(1)
M(2)-O3	2.085(2)	2.085(2)	2.023(1)
M(2)-O5	2.169(2)	2.183(2)	2.216(1)
M(2)-O5	2.108(2)	2.113(2)	2.024(1)
<M(2)-O>	2.079	2.084	2.034
$Vol_{M(2)}$	11.56	11.65	10.86
$BLD_{M(2)}$	2.03	2.09	3.12
$ELD_{M(2)}$	5.76	5.76	5.31
$OAV_{M(2)}$	83.95	84.35	94.70
$(e_u/e_s)_{M(2)}$	1.067	1.065	1.068
P(1)-O2 x2	1.536(2)	1.536(2)	1.538(1)
P(1)-O1 x2	1.537(2)	1.535(2)	1.541(1)
<P(1)-O>	1.536	1.535	1.539
$Vol_{P(1)}$	1.846	1.843	1.86
$BLD_{P(1)}$	0.04	0.05	0.09
$ELD_{P(1)}$	2.02	2.00	0.39
$TAV_{P(1)}$	18.75	18.69	8.81
P(2)-O6	1.535(2)	1.536(2)	1.522(1)
P(2)-O4	1.536(2)	1.533(2)	1.525(1)
P(2)-O5	1.537(2)	1.536(2)	1.555(1)
P(2)-O3	1.548(2)	1.545(2)	1.549(1)
<P(2)-O>	1.539	1.537	1.538
$Vol_{P(2)}$	1.86	1.86	1.87
$BLD_{P(2)}$	0.27	0.26	0.92
$ELD_{P(2)}$	0.89	0.82	0.39
$TAV_{P(2)}$	3.56	3.21	1.61

$$BLD = \frac{100}{n}\sum_{i=1}^{n}\frac{|(X-O)_i - (<X-O>)|}{(<X-O>)}\%,$$

n= amount of cation - anion bonds and X-O = cation - anion (oxygen) distance (Renner & Lehmann, 1986);

$$BLD = \frac{100}{n}\sum_{i=1}^{n}\frac{|(O-O)_i - (<O-O>)|}{(<O-O>)}\%,$$

n = amount of edges and (O-O) = oxygen - oxygen interatomic distance defining an edge of the octahedron (Renner & Lehmann, 1986); $OAV = \sum_{i=1}^{12}(\Theta_i - 90°)^2 /11$ with Θ_i = O-M-O bonding angle (Robinson *et al*., 1971); $TAV = \sum_{i=1}^{6}(\Theta_i - 109.57°)^2 / 5$ with Θ_i = O-T-O bonding angle (Robinson *et al*., 1971); e_u/e_s = ratio between unshared (e_u) and shared (e_s) octahedral edges (Toraya, 1981).

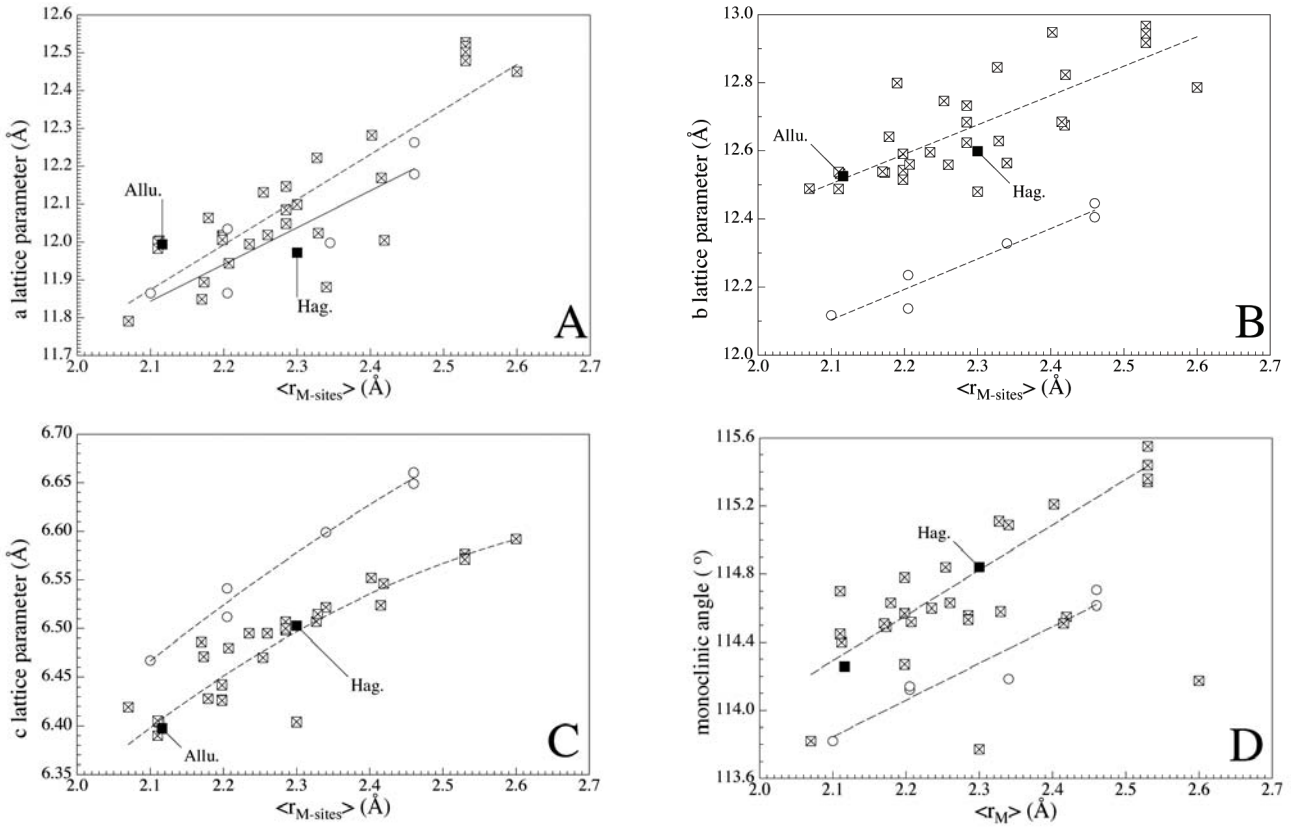

Fig. 2. Variation of lattice parameters with average M-site cationic radius in alluaudite-type compounds; filled squares = data of this study, open circles = protonated un-oxidized variants, crossed open squares = other literature data as referenced in Table 1.

into account the above findings, the filling of the A(2)′ site by sodium in hagendorfite compensates for the smaller A(1) cation radius and thus similar *a* and a slightly larger *b* lattice parameter are observed for it as compared to Buranga-pegmatite alluaudite.

Inspection of the lattice parameters in Fig. 2 also shows that the data for protonated - un-oxidized alluaudite compounds depart from the other literature data, forming their own trend. Leroux *et al*. (1995a, b) noted that H^+ atoms are bonded to the O(2) and O(4) oxygen atoms, straddled in the tunnels of the A(1) site (but at positions different from the A(1) cation, denoted A(1)′′ by Hatert *et al*., 2000). The formation of O(2)-H-O(4) hydrogen bonds brings a significant tightening of the cubic arrangement of oxygen atoms around A(1), accompanied by a decrease of the O(2)-O(4) bond distance from ≈ 3.0 Å in the non-protonated to ≈ 2.5 Å in the protonated forms (Leroux *et al*., 1995a). As this bond runs along *b*, this behaviour explains the distinctly smaller *b*-lattice parameters of the protonated alluaudite-type compounds depicted in Fig. 2b. Obviously, this shortening along *b* results in an increase along *c*, which is parallel to the tunnel-direction. It should be noted here, that on basis of bond lengths considerations the compound $NaFe_3(PO_4)_3$ of Corbin *et al*. (1986) also has to be a protonated alluaudite having all the iron in the divalent state, which then requires two H^+ for charge balance (Leroux *et al*., 1995a and Table 1).

3.2.2. Structural topology of hagendorfite at 298 K

A polyhedral representation of the hagendorfite crystal structure viewed down the *c* axis is shown in Fig. 3a. The main building units are $M(1)O_6$ and $M(2)O_6$ octahedra that share edges to form infinite kinked chains which form stacks parallel to the (1 0 1) plane (Fig. 3b). The chains consist of a pair of M(2) polyhedra, joined by a common edge and linked *via* edge-sharing to M(1) polyhedra. Equivalent chains are interconnected through the vertices of the P(1) and P(2) tetrahedra. The $P(1)O_4$ tetrahedra (Fig. 4) link two chains by sharing a pair of its oxygen atoms with one chain, the other pair with an adjacent chain, thereby forming buckled sheets parallel to the (0 1 0) plane. These are also described as "pleated" sheets in some literature references, *e.g.* Moore (1971).

The $P(2)O_4$ tetrahedra (Fig. 4b) connect three adjacent chains with each other. Two of the tetrahedral vertices are common to one chain; the third one is shared with an adjacent chain. The fourth vertex of the tetrahedron points outward away from the buckled sheet and is shared with a third M(1)M(2)-octahedral chain. It is this outward pointing fourth corner of the $P(2)O_4$ tetrahedron, which interconnects individual (1 0 1) sheets. This complex arrangement of distorted octahedra and tetrahedra produces an open framework structure having two crystallographically different channels parallel to the *c* direction,

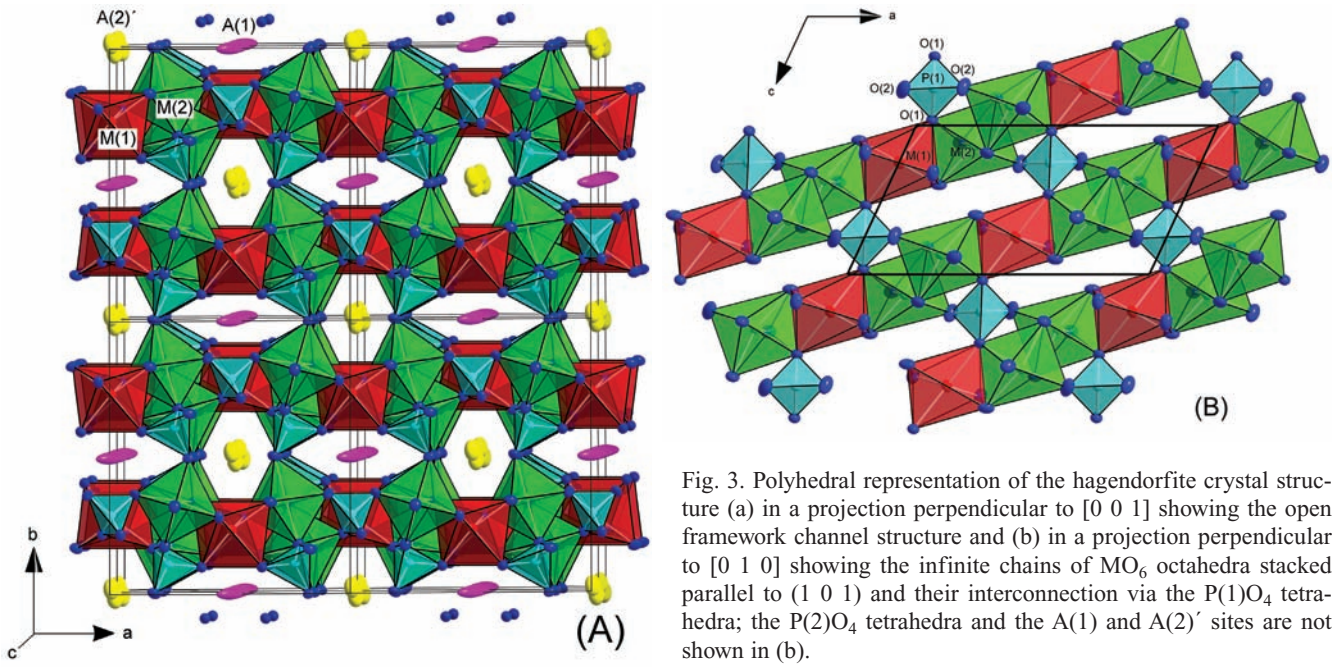

Fig. 3. Polyhedral representation of the hagendorfite crystal structure (a) in a projection perpendicular to [0 0 1] showing the open framework channel structure and (b) in a projection perpendicular to [0 1 0] showing the infinite chains of MO_6 octahedra stacked parallel to (1 0 1) and their interconnection via the $P(1)O_4$ tetrahedra; the $P(2)O_4$ tetrahedra and the A(1) and A(2)´ sites are not shown in (b).

containing the A(1) and the A(2)´ sites. The large cations such as Na^+, Ag^+ or Ca^{2+} reside in these channels.

The M(1) site is six-fold coordinated with the M(1)-O bond lengths ranging between 2.211(2) Å and 2.236(2) Å. The large bond lengths support the assumption that the large Mn^{2+} cation is occupying this position. Using the widely accepted ionic radius of 1.40 Å for oxygen and subtracting it from the average M(1)-O bond length of 2.223 Å results in an average experimental ionic radius of 0.823 Å for the M(1) cation, which perfectly fits the one given for Mn^{2+} by Shannon & Prewitt (1969) with 0.82 Å. If ferrous iron would be present on M(1), shorter M(1)-O bond lengths would be expected, even if the Fe^{2+}-O bond lengths on M(1) site in alluaudite are larger than in other Fe^{2+} bearing phosphates or in silicates. In alluaudite-type $NaFe^{2+}_3(PO_4)(H_2PO_4)_2$ the Fe^{2+} M(1)-O bond lengths range between 2.123(3) and 2.217(3) Å, average value 2.175 Å (Corbin *et al*., 1986), in $Na_2Fe^{2+}_{1.74}Fe^{3+}_{1.26}(PO_4)_3$ they range between 2.142(6) and 2.229(6) Å, average value 2.195 Å (Hatert *et al*., 2005), in $NaFe_{3.67}(PO_4)_3$, the Fe^{2+} M(1)-O bond lengths are between 2.196(3) Å and 2.218(3) Å, average value 2.192 Å. Compared to these, the iron phosphate $Na_{0.1}Fe_7(PO_4)_6$ having one 6-fold coordinated Fe^{2+} site shows average Fe^{2+}-O bond lengths of 2.179(1) Å (Redhammer *et al*., 2004), in the hydrous iron phosphate barbosalite $Fe^{2+}Fe^{3+}_2(PO_4)_2(OH)_2$ it is 2.112(2) Å only

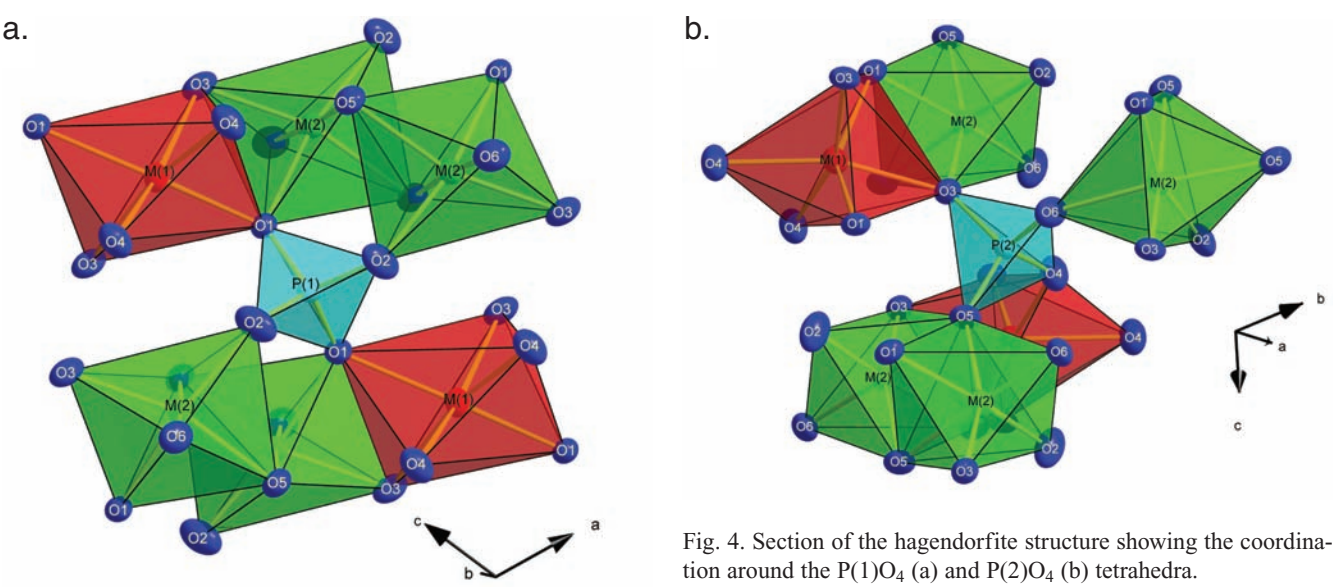

Fig. 4. Section of the hagendorfite structure showing the coordination around the $P(1)O_4$ (a) and $P(2)O_4$ (b) tetrahedra.

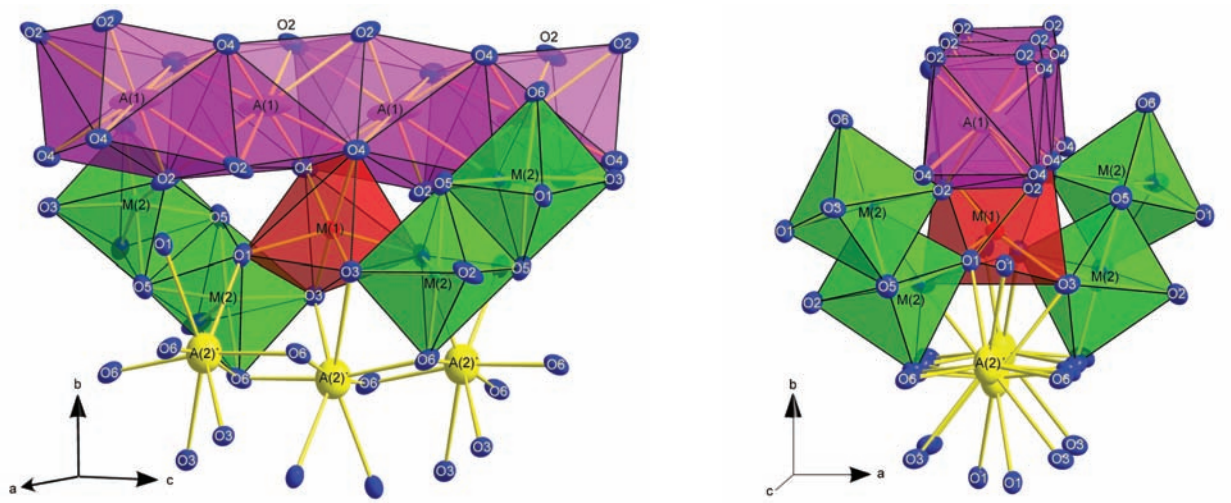

Fig. 5. Section of the hagendorfite structure showing the connectivity of A(1), A(2)´, M(1) and M(2) in two different views (a) almost along [1 0 1] and (b) almost along [0 0 1]. P atoms are not shown for clarity.

(Redhammer *et al*., 2000). Bond length - bond strength calculations for hagendorfite (Brese & O'Keeffe, 1991) reveal a bond valence sum of s = 1.86 valence units (vu) for the M(1) site in a quite reasonable agreement with the expected value of 2.0 for Mn^{2+}.

The deviation of individual bond lengths from their mean value (bond lengths distortion, BLD; Renner & Lehmann, 1986) is small for the M(1) site in hagendorfite (BLD = 0.40 %) and the M(1) site appears as a quite regular octahedron. Similar was found for natural and synthetic Na-Mn-Fe bearing alluaudites by Hatert *et al*., (2004) giving values of BLD ranging from 1.22 % to 2.05 % for the M(1) site. However, looking on the octahedral angle variance OAV (Robinson *et al*., 1971) it is found that the M(1) octahedron exhibits a distinct bond angle variance with the quadratic OAV being 209.7(1)°. It is the large O(1)-M(1)-O(4) bond angle (115.43(8)°), which is mainly responsible for this large OAV. Also, the edge length distortion (ELD, Renner & Lehmann, 1986) is large with ELD = 8.77 %. As expected, the two octahedral edges [O(1)-O(3)], shared with neighbouring M(2) sites, are distinctly shorter (2.668(2) Å) as compared to the unshared ones. Additionally the M(1) octahedron joins a common edge with two neighbouring A(1) sites (Fig. 5), this O(4)-O(4)

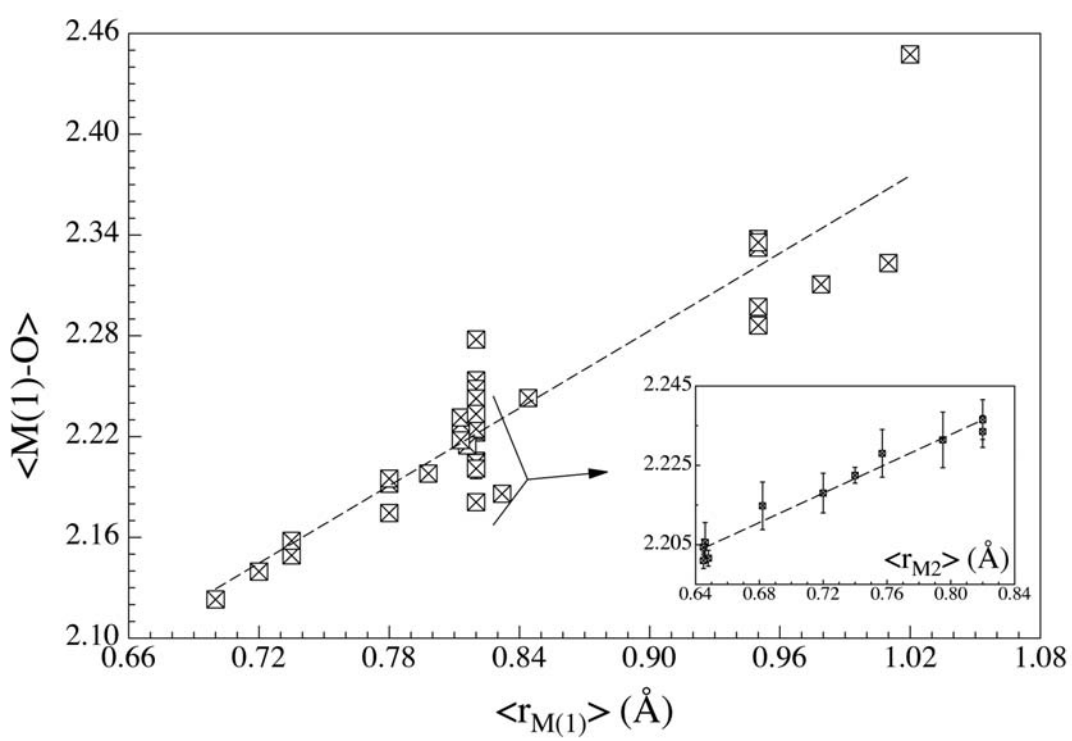

Fig. 6. Variation of average M(1)-O bond lengths with the size of the M(1) site cation for various alluaudite type compounds. The inset displays the dependence of <M(1)-O> on the average M(2) site cationic size $<r_{M(2)}>$.

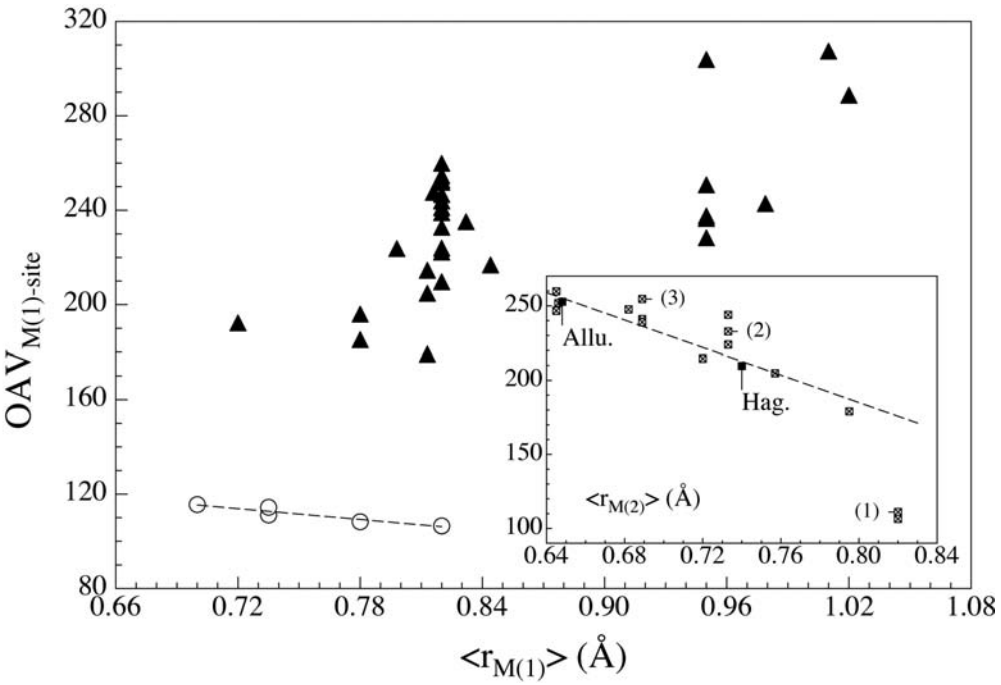

Fig. 7. Octahedral angle variance of the M(1) site in different alluaudite-type compounds *vs.* average ionic radius of the M(1) site. The inset displays the variation of OAV with the average M(2)-site ionic radius for samples having Mn^{2+} on M(1) exclusively; (1) = protonated, un-oxidized samples (2) Ag containing samples of Daidouh et al. (2002), (3) Na-Li substitution of Hatert et al. (2002).

edge is also rather short (2.815(2)) Å. The largest octahedral edge is the O(1)-O(4) edge with 3.768(2) Å, which is opposite to the large O(1)-M(1)-O(4) bond angle. The ratio of the average of unshared (e_u) to shared (e_s) edges can be used as a measure of polyhedral distortion too (e_u/e_s, Toraya, 1986). It is 1.21 for the hagendorfite M(1) octahedron. For comparison, regular octahedra as found in chain and sheet silicates have e_u/e_s values ranging between 1.03-1.08 for the clinopyroxenes (Redhammer & Roth, 2004) and 1.08-1.012 for trioctahedral micas (Redhammer & Roth, 2002).

In Buranga alluaudite, the M(1) site is occupied by Mn^{2+} also. The M(1)-O bond lengths range between 2.179(1) and 2.238(1) Å, the average value is 2.202 Å. This is slightly smaller than in hagendorfite but in perfect agreement with the data of Hatert *et al*., (2000) for the idealized synthetic alluaudite $NaMnFe_2(PO_4)_3$ (<M(1)-O> = 2.204 Å) and with the data given by Moore (1971). Plotting average M(1)-O values *vs.* the average M(1)-site ionic radii (Fig. 6) shows a positive correlation, similar to the one observed by Hatert (2002). It also is evident, that the average M(1)-O bond length is not solely a function of the M1-site cationic radius. This is evident for the several alluaudite-type compounds with the the M(1) site being occupied by Mn^{2+} (0.82 Å). Taking samples having Mn^{2+} on M(1) and a similar A-site composition (1 Na^+) a positive correlation can be established between the mean M(1)-O bond lengths and the average radius of the M(2) cation. This correlation is not surprising as M(1) and M(2) sites are tightly connected to each other within the buckled M-site chain (Fig. 4, 5). Furthermore, for constant M(1) and M(2) site composition, the average M(1)-O bond lengths also varies with changing A-site composition.

The M(1)-octahedron in Buranga alluaudite exhibits a larger polyhedral distortion, as compared to hagendorfite. A rough correlation exists between the size of the M(1)-cation and the octahedral angle variance, meaning that the larger the M(1) cation, the larger the polyhedral distortion (Fig. 7). However, it becomes evident for the samples with exclusively Mn^{2+} on M(1) that factors other than the M(1) cation influence the polyhedral distortion of the oxygen coordination polyhedron around M(1). Again a good correlation can be found between $OAV_{M(1)}$ and the size of the M(2) cation. It is evident that the angular distortion of the M(1) site decreases as the M(2) ionic radius approaches the value of the M(1) cation. Thus the lower angular distortion of hagendorfite - as compared to alluaudite - is due to the fact that the radius of the M(1) cation is more similar to the one of the M(2) site cation in alluaudite. It is worth noting that the protonated, un-oxidized samples with the M(1) and M(2) sites being occupied by the same kind of cation have distinctly lower angular distortion as compared to the other compounds, supporting the above consideration. However, only samples with predominantely sodium on the A-sites plot well along a linear trend. Substituting Na^+ by Ag^+ in $Na_2FeMn_2(PO_4)_3$ as done by Daidouh *et al*. (2002) alters the angular distortion of the M(1) site too, with the Ag rich samples exhibiting a more distorted environment. Similar observations have been made for the $Na_{1-x}Li_x$ substitution in $NaCdIn_2(PO_4)_3$ (Hatert *et al*., 2002).

The M(2) site of hagendorfite is also six-fold coordinated with the M(2)-O bond lengths ranging between 1.983(2) Å and 2.183(2) Å, average M(2)-O = 2.084 Å. Individual and average bond lengths agree well with those expected for a site having a mixed occupation of Fe^{2+} and Fe^{3+}. However, they are too short for considerable amounts of Mn^{2+} occupying this site. As chemical analysis has shown, the M(2) site contains 0.09 atoms per formula unit Mn^{2+}. Bond valence calculations for the M(2) site cation also suggest a mixed occupation with di- and trivalent iron

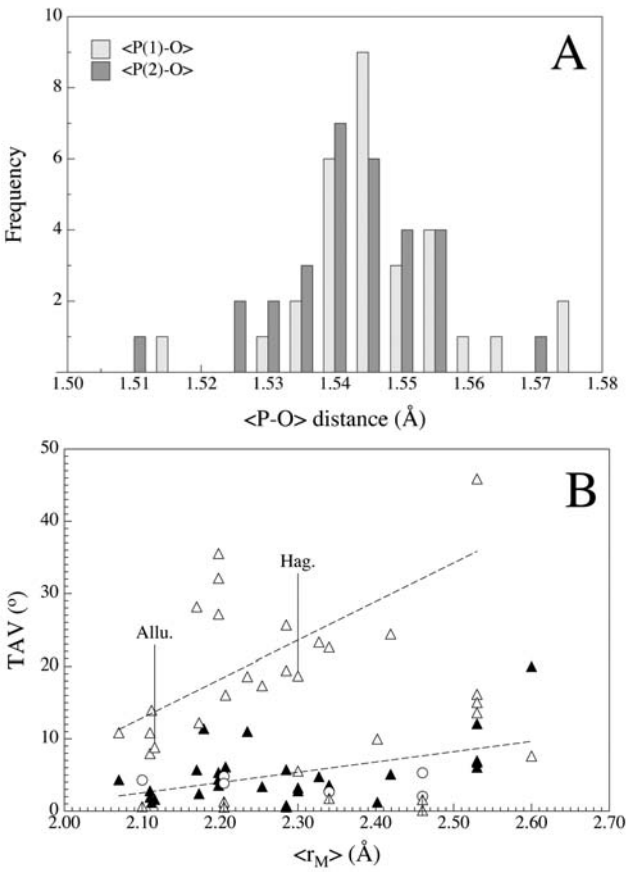

Fig. 8. (a) Histogram analysis of the occurrence of average P-O bond length in alluaudite type compounds; (b) Tetrahedral angle variance *vs.* the average M-site cationic size ($\langle r\rangle_{M1} + 2*\langle r\rangle_{M2}$): open symbols representing data for the (P1) site, filled symbols those for the P(2) site.

as the bond valence sum s = 2.37 vu. The BLD = 2.09 % is larger than for the M(1) site, however, the angular distortion OAV is distinctly lower. Again this is in good agreement with the recent findings of Hatert *et al*. (2004) giving BLD values of 2.79 to 4.97 % for their samples. The M(2) polyhedron shares two of its edges with neighbouring polyhedra, one with a neighbouring M(2) and one with a neighbouring M(1) polyhedron. All of its oxygen atoms are shared with PO_4 tetrahedra. Like the OAV, the edge length distortion in hagendorfite is smaller for the M(2) site (ELD = 5.76 %) as compared to the M(1) site. Also the ratio e_u/e_s is distinctly smaller with e_u/e_s = 1.06 again showing the M(2) octahedron to be much more regular than M(1). In Buranga-pegmatite alluaudite with predominately Fe^{3+} at the M(2) site the average bond length is shorter (M(2)-O = 2.035 Å) as the radius in hagendorfite. Using 1.40 Å as the radius of the oxygen atom (Shannon & Prewitt, 1969), an experimental ionic radius of 0.635 Å for the M(2) site cation is obtained which is in good agreement with the radius of Fe^{3+} (0.645 Å, Shannon & Prewitt, 1969). However, it is interesting to note that one of the two M(2)-O5 bond lengths in alluaudite (2.216(2) Å) is larger compared to the corresponding bond lengths in hagendorfite (2.183(2) Å) even if alluaudite hosts the smaller M(2) cation. This is due to the enhanced electrostatic repulsive forces between the neighbouring M(2) cations Fe^{3+}-Fe^{3+}, leading also to an increase in the M(2)-M(2) interatomic distance from 3.165(2) to 3.205(1) and an increase of the M(2)-O(5)-M(2) bond angle from 94.87(8)° to 97.57(8)° in hagendorfite and alluaudite, respectively. All other M(2)-O bond lengths are smaller in alluaudite as compared to hagendorfite, as would be expected. The M(2) site in alluaudite exhibits a larger polyhedral distortion than in the title compound with BLD = 3.12 % and the OAV = 94.70°.

The PO_4 tetrahedra are regular in both compounds investigated here. The P(1) tetrahedron shows almost identical bond lengths with BLD parameters < 0.1 % for hagendorfite and alluaudite. The average P(1)-O bond lengths are 1.535 and 1.539 Å, respectively. The edge lengths distortion ELD however is quite large in hagendorfite (ELD = 2.00 %). This is mainly due to the large O(1)-O(2) distance of 2.579(2) Å between the pair of oxygen atoms belonging to one M-site chain and shared with two different M(2) sites (Fig. 4a). The distances between oxygen atoms of the $P(1)O_4$ tetrahedron, forming edges connecting two different chains are much smaller. In contrast, alluaudite shows more regular $P(1)O_4$ tetrahedral edge lengths with ELD = 0.38 %. Here, all tetrahedral edges of the P(1) site are within 2.500(2) Å and 2.522(2) Å and the O(1)-O(2) edge shared with one and the same M-site chain is shorter by ≈ 0.08 Å as compared to hagendorfite. The longer O(1)-O(2) edge length in hagendorfite probably is the result of the larger size of the M(2) site due to the presence of Fe^{2+} as compared to Fe^{3+} in alluaudite. The larger variation of edge lengths in hagendorfite is also reflected in a quite large tetrahedral angle variance, TAV (Robinson *et al*., 1971) with TAV = 18.7°. Alluaudite shows a much more regular bond angle environment around P(1) with TAV = 8.81°. Bond valence calculations (Brese & O´Keeffe, 1991) show that the P(1) atom is slightly "underbonded" (bond valence sum s = 3.82 valence units, vu), in hagendorfite whereas the O(1) and O(2) oxygen atoms are over-bonded (s = 2.08 and 2.07 vu respectively). Similar values were found for alluaudite. Just as P(1), P(2) is also "undersaturated" in charge, both in hagendorfite and in alluaudite. This has also been observed by several authors before (*e.g.* Leroux *et al*., 1995a, b) for other alluaudite-type compounds. All of the oxygen atoms coordinating the P(2) atom are slightly under-saturated in charge. In both compounds the P(2) tetrahedron (Fig. 4b) is more regular than the P(1) oxygen environment. This is revealed especially by a smaller deviation of the bond angles from their ideal value (TAV = 3.21° and 1.61° in hagendorfite and alluaudite, respectively) and small ELD parameters (0.81 % and 0.38% respectively). The average P-O bond lengths in alluaudite-type compounds vary between 1.505 and 1.575 Å, the most abundant values are found in a class between 1.545 and 1.550 Å for the P(1) site and between 1.540 and 1.545 Å for the P(2) site (Fig. 8a). The data found here are slightly smaller but are fitting well within the most populated groups observed in histogram analysis of the different mean P-O bond lengths (Fig. 8a). It should also be noted that the broad distribution is also due to the

fact that structural parameters for more than half of the alluaudite-type compounds compiled here are from Rietveld refinement of X-ray powder diffraction data and that these are less accurate than those obtained by single crystal X-ray diffraction. The observation that the P(2) site, sharing its vertices with three different M-site chains, is less distorted, is a more general observation, which holds true for most of the alluaudite-type compounds. Plotting the tetrahedral angle variance *vs.* the average of the M-site cationic radius (as defined above), reflecting changing chemical composition, it is found that a rough positive correlation seems to exist (Fig. 8b). This is more evident for the P(2) site. The fact that increasing the M-site cationic radius introduces increasing angular distortion to the tetrahedral sites is not unexpected as especially the P(1) site shares two of its vertices with one and the same chain and the tetrahedron has to react to an increase in M-site volume due to an increase of the M-site cation radius (Fig. 4a). It is also evident from Fig. 8b that the protonated, un-oxidized samples generally have low tetrahedral bond angle distortion and that P(1) and P(2) sites are similar in terms of TAV.

The A(1) site, hosting both Na^+ and Ca^{2+} in hagendorfite, is located in channel 1 of the alluaudite-type structure at ($^1/_2$, 0, 0) and (0, $^1/_2$, 0). It is coordinated by eight oxygen atoms forming a distorted cube. These cubes share two common faces with each other forming the channel parallel to the *c* direction. Furthermore, two of the edges are shared with neighbouring $M(1)O_6$ octahedra. The A(1)-O bond lengths range between 2.286(2) Å and 2.970(2) Å, average value 2.548 Å. The experimental cationic radius for the A(1) cation is 1.148 Å (with rO^{2-} = 1.40 Å), which is close to the value of 1.16 Å given by Shannon & Prewitt (1969) for $^{VIII}Na^+$ (with VIII as the coordination number). The cation radius for $^{VIII}Ca^{2+}$ is given as 1.12 Å. So the average A(1)-O bond length reflects nicely the occupation of this site by Ca^{2+} and Na^+. Bond-strength - bond-valence calculations give a valence sum s = 1.38, which can be seen as further evidence that on A(1) not only Na^+ but also Ca^{2+} and Mn^{2+} are present. The A(1)-O bond lengths in hagendorfite are close to the ones in alluaudite and both plot well into the range of A(1)-O bond lengths found in the literature for the different alluaudite-type compounds. A plot of the average ionic radius of the A(1) site *vs.* the average A(1)-O bond length shows a weak positive correlation but also exhibits that the average ionic radius of the M-site cations play an even more prominent role in determining the size of the A(1)-O bond lengths. Along with the M(1) cation size, the M-site cationic radius also increases the average A(1)-O bond length (Fig. 9).

Both in hagendorfite and in alluaudite the A(2)′ site is occupied. For alluaudite this means that the original A(2) position at (0, 0, 0) proposed by Moore (1971) is empty. Even in alluaudite, sodium is found on the more frequently occupied A(2)′ position. Among all the alluaudite-type compounds compiled here, there is not a single one in which the original A(2) position is occupied. Only for the compound $Cu_{1.35}Fe_3(PO_4)_3$ an occupied A(2) position was reported (Warner *et al*., 1993). We therefore conclude that this position is not a regular cationic position in alluaudite-type compounds. In hagendorfite the A(2)′ position is surrounded by eight oxygen atoms, forming a 4+4 oxygen coordination with 4 short and 4 long bonds. The inner oxygen environment of the Na^+ atoms is nearly square planar with bond lengths between 2.418(2) and 2.574(2) Å. The longer bonds are between 2.801(3) and 2.920(2) Å. The general morphology of the A(2)′ site was described by Hatert *et al*. (2000) to correspond to the gable disphenoid

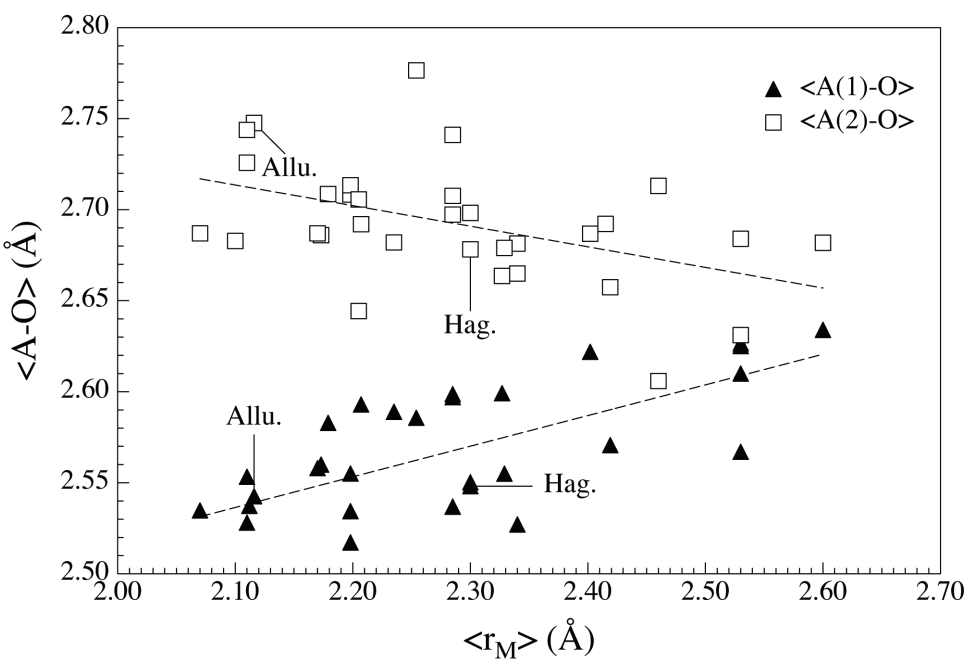

Fig. 9. Average A(1)-O and A(2)-O bond lengths *vs*. the average M-site cations in different alluaudite type compounds.

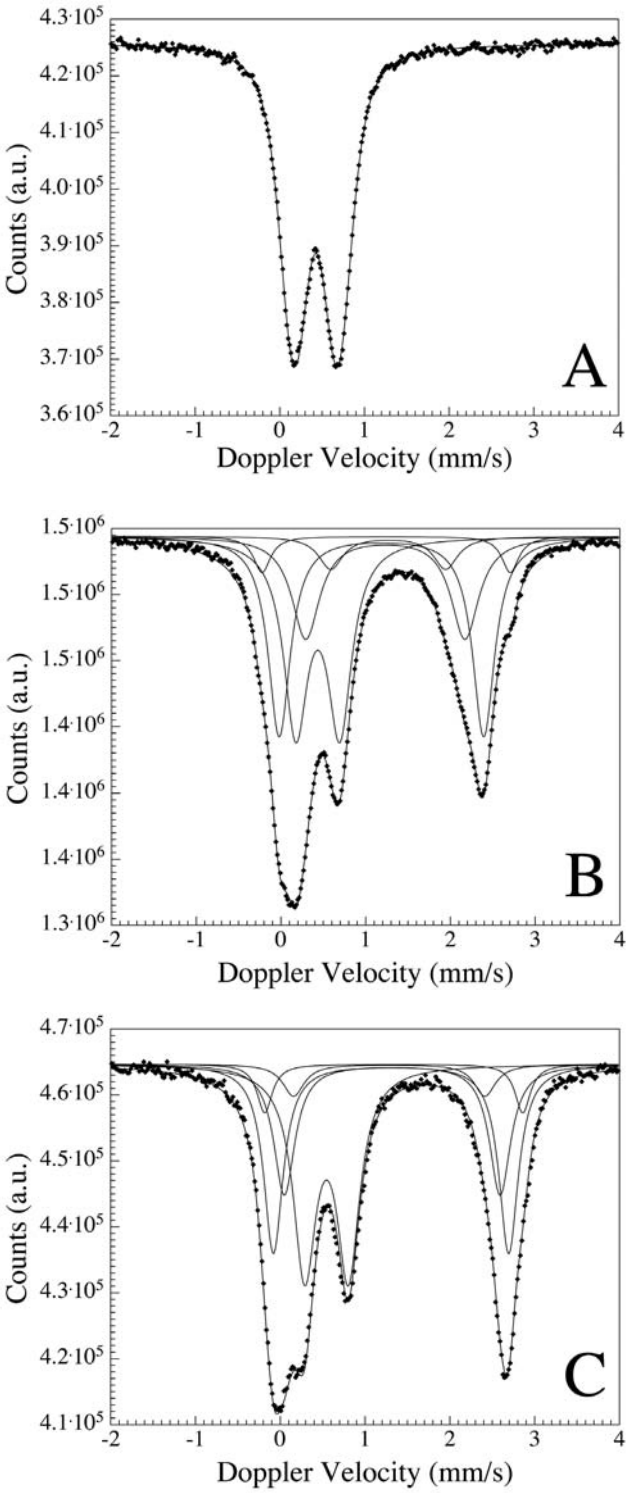

Fig. 10. ^{57}Fe Mössbauer spectra of alluaudite s.s. at 298K (a) and of hagendorfite at 298 K (b) and 80 K (c).

in the wyllieite structure. Bond valence calculations show a bond valence sum of s = 1.03 vu for the A(2)′ position hagendorfite, a clear evidence for the exclusive occupation by Na^+. The long-distant A(2)-O bonds only contribute 0.05 valence units each to the valence sum of sodium. As for the A(1) site, the average A(1)-O bond length is not only a function of the average A(2)′ site cation but also depends on the radius of the M-site cations. This is evident from Fig. 9.

3.2.2. Structural changes upon cooling

Hagendorfite has also been investigated at 100 K but no change in symmetry was observed. There are no significant changes within the general topology of the hagendorfite structure between 100 K and 300 K. The lattice parameters *a*, *b* and *c* decrease with temperature, most pronounced along the *b* direction, which shrinks by 0.35 % and followed by the *a* direction (0.19 %). Least accessible to cooling is the *c* direction which decreases by 0.09 % only. Among the structural parameters the average A(1)-O and A(2)′-O bond lengths are shorter by ≈ 0.09 Å at 100 K (changes by ≈ 0.35 %). Also for the strongly distorted M(1) site a distinct shortening of the bond lengths is observed which amounts 0.09 Å. The polyhedral distortion tends to increase. The average bond length at the more regular M(2) site only shrinks by 0.05 Å and for the tetrahedral sites, only minor changes are observed. Here the average P(1)-O and P(2)-O bond lengths appear to be slightly longer at 100 K as compared to room temperature, this also applies to the polyhedral volume of the P-sites. However these changes are within one standard deviation. The observed bond length alterations are consistent with the more general observation that large distorted polyhedra show large bond length alterations, whereas small regular polyhedra behave as rigid units upon changes in one or more parameters of state.

3.3. ^{57}Fe Mössbauer spectroscopy

The Mössbauer spectrum of the Buranga-pegmatite alluaudite shows two symmetric, narrow split absorption lines which can be adequately fitted with one doublet (Fig. 10a). This leads to ^{57}Fe hyperfine parameters which are typical for high-spin ferric iron in octahedral coordination (Table 6). No evidence is found for a second Fe^{3+} doublet or that there is a distinct distribution of Fe^{3+} quadrupole splittings. For the $(Na_{1-x}Li_x)MnFe_2(PO_4)_3$ series Hermann *et al*. (2002) found small amounts of Fe^{2+} on M(2) and they needed two doublets to adequately fit the ferric iron absorption contribution (and two for Fe^{2+}). This behaviour was interpreted as an evidence for a next-nearest neighbour (NNN) effect. Also, Hidouri *et al*. (2004b) observed two ferric iron doublets for $Na_4CaFe_4(PO_4)_6$, which they assigned to next nearest neighbour effects due to the mixed occupation of the M(1) site with Na^+ and Ca^{2+}. However, such NNN-effects are not to be expected in the alluaudite sample studied here as the M(1) site is occupied by Mn^{2+} only, and all the iron, filling the M(2) site, is exclusively in the trivalent state. The small amount of Mg^{2+} and Mn^{2+} (see EMPA) on M(2) obviously does not lead to clearly detectable NNN-configurations. However, it should be noted that during evaluation of the spectrum with the quadrupole splitting distribution (QSD) model with one component for Fe^{3+}, a rather large Gaussian width of σ = 0.21 mm/s was observed which is an indication of a small

Table 6. ^{57}Fe Mössbauer parameters of alluaudite, hagendorfite as extracted from refining the thickness corrected Mössbauer spectra using Lorentzian shaped quadrupole doublets. Mössbauer parameters for selected alluaudite-type compounds from literature are included for comparison.

Sample	T (K)	δ (mm/s)	Δ (mm/s)	Γ (mm/s)	A (%)	Site	Ref.
Alluaudite *s.s.*	298	0.43	0.52	0.13	100	Fe^{3+}M(2)	(a)
Hagendorfite	80	0.55	0.52	0.16	37.1(6)	Fe^{3+}M(2)	(a)
		1.31	2.78	0.14	29.3(8)	Fe^{2+}M(2)	
		1.32	2.55	0.15	22.3(9)	Fe^{2+}M(2)	
		1.29	2.26	0.15	5.5(11)	Fe^{2+}M(2)	
		1.34	3.04	0.12	5.9(9)	Fe^{2+}M(2)	
	150	0.52	0.52	0.17	36.6(6)	Fe^{3+}M(2)	(a)
		1.28	2.69	0.13	30.5(9)	Fe^{2+}M(2)	
		1.28	2.45	0.16	21.9(7)	Fe^{2+}M(2)	
		1.29	2.00	0.19	5.7(9)	Fe^{2+}M(2)	
		1.29	3.00	0.13	5.2(8)	Fe^{2+}M(2)	
	298	0.43	0.53	0.17	36.1(7)	Fe^{3+}M(2)	(a)
		1.19	2.42	0.15	31.5(9)	Fe^{2+}M(2)	
		1.23	1.89	0.20	22.5(11)	Fe^{2+}M(2)	
		1.23	1.40	0.19	5.0(9)	Fe^{2+}M(2)	
		1.24	2.93	0.12	5.0(10)	Fe^{2+}M(2)	
$NaFe_{3.67}(PO_4)_3$	298	1.22	2.08	0.21	57.3	Fe(1)	(b)
		1.24	2.40	0.18	28.6	Fe(2)	
		0.50	0.38	0.17	14.1	Fe(3)	
$Na_4CaFe_4(PO_4)_6$	293	0.432	0.438	0.14	49.6	Fe^{3+}M(2)	(c)
		0.430	0.611	0.14	50.4	Fe^{3+}M(2)	
$NaMnFe_2(PO_4)_3$	295	0.428	0.520	0.15	17.8	Fe^{3+}M(2)	(d)
			0.77			Fe^{3+}M(2)	
		1.0253	2.71	0.21	82.2	Fe^{2+}M(2)	
			2.09			Fe^{2+}M(2)	
$Na_2Mn_2Fe(PO_4)_3$ #1	295	0.424	0.92	0.15	50	Fe^{3+} M(2)	(e)
		0.424	0.60	0.15	50	Fe^{3+} M(2)	
$NaMnFe_2(PO_4)_3$ #2	295	1.250	1.99	0.28	3.8	Fe^{2+} M(2)	(e)
		1.250	2.65	0.28	15.2	Fe^{2+} M(2	
		0.430	0.78	0.17	16.2	Fe^{3+} M(2)	
		0.430	0.52	0.17	64.8	Fe^{3+} M(2)	
$NaMnFe_2(PO_4)_3$ #3	298	1.217	2.21	0.27	1.0	Fe^{2+} M(2)	(e)
		1.217	2.47	0.27	9.0	Fe^{2+} M(2	
		0.433	0.85	0.17	9.0	Fe^{3+} M(2)	
		0.433	0.55	0.17	81.0	Fe^{3+} M(2)	
$Na_2MnFe_2(PO_4)_3$ #4	298	1.172	2.13	0.22	27.03	Fe^{2+} M(2)	(e)
		1.172	2.34	0.22	24.96	Fe^{2+} M(2	
		0.459	0.57	0.17	24.96	Fe^{3+} M(2)	
		0.459	0.34	0.17	23.04	Fe^{3+} M(2)	

δ = isomer shift relative to α - Fe, Δ = quadrupole splitting, Γ = half width at half maximum of the Lorentzian-shaped lines. Estimated standard deviation for δ, Δ and Γ ≤ 0.01 mm/s.
Ref.: (a) this study, (b) Korzenski *et al*. (1998), (c) Hidouri *et al*. (2004b), (d) Hermann *et al*. (2002), (e) Hatert *et al*. (2004).

QSD around the maximum quadrupole splitting value of 0.52(1) mm/s. The Mössbauer parameters found for Fe^{3+} in alluaudite are in good agreement with values given in literature for Fe^{3+} on M(2) in other alluaudite-type compounds (Table 6).

In contrast to the quite simple appearance of the alluaudite *s.s.* Mössbauer spectrum, the spectrum of hagendorfite is complex. At room temperature it consists of 3 broad resonance absorption lines which result from both ferric and ferrous iron contributions (Fig. 10b). Interestingly the Fe^{3+} contribution seems to show a rather small line width (Γ/2 ≈ 0.16 mm/s) without any asymmetric line broadening. This is indicative of a quite uniform local distortion environment around the Fe^{3+} probe nuclei. The Fe^{2+} contribution however is broad, showing shoulders at the high velocity peak at ≈ 2.35 mm/s which are visible even by visual inspection of the spectrum. At least 4 doublets (or components) are necessary to model the Fe^{2+} resonance absorption reasonably. Thus, for the evaluation the 298 K hagendorfite Mössbauer spectrum a model with four Fe^{2+}, but only one Fe^{3+} doublet was chosen. With this assumption an almost perfect refinement is possible (Fig. 10b). The

^{57}Fe Mössbauer parameters obtained from this refinement are given in Table 6. The relative intensities of the Fe^{2+} components show that there are two main components which account for almost 85 % of the Fe^{2+}, the two other Fe^{2+} components are equal but low in relative intensity. It should, however, be noted here that the omission of one or both of the two low intensity Fe^{2+} doublets results in unacceptable refinements with distinct misfits predominantely at the high velocity Fe^{2+} peak at ≈ 2.35 mm/s. It should also be noted that adding a second doublet for ferric iron did not improve the quality of the refinement but lead to unstable refinements and to problems with convergence. The ^{57}Fe Mössbauer parameters of such a second Fe^{3+} doublet are almost identical to the ones of the first one. The model developed for the 298 K spectrum was successfully used to refine the spectra collected at 150 K and 80 K also. Results are compiled in Table 6, the spectrum at 80 K is displayed as an example in Fig. 10c. With decreasing temperature the spectral resolution slightly decreases as individual Fe^{2+} doublets overlap more closely.

The question as to the physical meaning of such a 5 doublet needs to be addressed. Obviously, the doublet with the small isomer shift of 0.41 mm/s and a quadrupole splitting of 0.50 mm/s has to be ascribed to ferric iron on the M(2) site. The ^{57}Fe hyperfine parameters of Fe^{3+} in hagendorfite are very close to the ones found for alluaudite *s.s.* (Table 6) and also fit well into the range of parameters found in other synthetic alluaudite-type compounds. The fact that there is no asymmetric line broadening for ferric iron indicates a lacking variation of the local (electronic and/or geometric) distortion around the Fe^{3+} cations on M(2). Possibly local clusters are formed in which a central Fe^{3+} cation is neighboured by Mn^{2+} (M(1)) and Fe^{3+} (M(2)).

Things are more complicated for Fe^{2+}. It should be recalled that there are two crystallographic sites in the hagendorfite structure which may host Fe^{2+}, the M(1) and the M(2) site. The present results for Fe^{2+} may be interpreted in terms of a distribution of Fe^{2+} over M(1) and M(2) sites. Because of an inverse correlation between the deviation from ideal geometry of an octahedron and the Fe^{2+} quadrupole splitting (Ingalls, 1964; Dowtey & Lindsley, 1973) low quadrupole splitting values should be expected for Fe^{2+} on M(1) with its larger polyhedral distortion. The two Fe^{2+} doublets with lowest quadrupole splitting of 1.40(1) and 1.89(1) mm/s have relative area fractions of 7.1(8) % and 22.4(6) % respectively. These area fractions correspond to 0.14 and 0.44 Fe^{2+} atoms per formula unit. Even assigning only the innermost Fe^{2+} doublet to the M(1) site corresponds to quite a large amount of Fe^{2+}; attributing the 1.89(1) mm/s doubl*et al*so to M(1) would mean that almost 60 % of the M(1) site would be occupied by Fe^{2+}. This is assumed to be unrealistic for the Buranga-alluaudite sample of this study. Furthermore, the structural data with the large average M(1)-O bond length indicate that only minor amounts of Fe^{2+} are to be expected. So at the very most the innermost doublet presumably corresponds to Fe^{2+} on M(1) and the remaining 3 Fe^{2+} components have to be assigned to the M(2) site, implying the next nearest neighbour (NNN) effects have to be invoked to explain them. We prefer not to assign any of the ferrous iron components to the M(1) site, but rather assume that all 4 components correspond to Fe^{2+} on M(2) and arise from NNN-effects due to different occupation of neighbouring M(2) sites. However, only two different NNN environments do exist when taking into account the M(2) sites, namely (Fe^{2+}-Fe^{2+}) and (Fe^{2+}-Fe^{3+}) configurations, explaining only two components. Thus the A(1) site cations, sharing an edge with the M(1) site, probably also have some influence due to the different charges and ionic radii of the Na^{+}, Ca^{2+} and Mn^{2+} cations hosted on A(1). Taking this into account, several different NNN-configurations are now possible. The most probable one is a Fe^{2+}-(Fe^{2+}, Ca^{2+}, Ca^{2+}) configuration, followed in probability by a Fe^{2+}-(Fe^{3+}, Ca^{2+}, Ca^{2+}) configuration. Due to the higher charge of Fe^{3+}, the latter will impose a larger distortion on the local electronic/geometric environment around Fe^{2+}, thus leading to a smaller quadrupole splitting. From this, the most intense Fe^{2+} component, having a quadrupole splitting of 2.42 mm/s, most probably corresponds to a (Fe^{2+}, Ca^{2+}, Ca^{2+}) - NNN configuration, whereas the second most intense component with a smaller QS of 1.89(1) mm/s can be ascribed to a (Fe^{3+}, Ca^{2+}, Ca^{2+}) configuration. The two remaining components may arise from (Fe^{2+}, Ca^{2+}, Na^{+}) and (Fe^{2+}, Ca^{2+}, Mn^{2+}) configurations, however, other ones involving Fe^{3+} are also possible. Configurations involving Na^{+}-Na^{+} and Mn^{2+}-Mn^{2+} pairs are assumed to play a minor role due to the low concentrations of the latter cations on A(1).

The assumption of different NNN configurations being responsible for the line broadenings is supported by the fact that the relative area ratios of individual Fe^{2+} components do not change distinctly with temperature but are similar at all temperatures investigated. However, as it is expected from theory, cooling to low temperatures causes an increase of the isomer shift values as a result of the second order Doppler shift. A distinct increase of the quadrupole splitting of Fe^{2+} towards lower temperatures is also observed (Table 6). On the other hand, only minor changes are observed for the quadrupole splitting of Fe^{3+}. These changes led to a better resolution of the spectra at 298 K as compared to 80 K (as mentioned above).

4. Conclusions

(1) Hagendorfite is isostructural to alluaudite. It exhibits space group *C*2/*c* both at 298 K and 100 K. Both in the title compound and in alluaudite *s.s.* from Buranga pegmatite, the A(2)' site at (0, y, $^1/_4$) with y ≈ 0 is occupied. This is in contrast to the findings of Moore (1971), who proposed that in alluaudite *s.s.* the A(2) at (0, 0, 0) would be occupied. A survey of literature data showed that it is the A(2)' site, but not the originally proposed A(2) site, which is occupied in alluaudite-type compounds.

(2) The lattice parameters of alluaudite-type minerals correlate with the average M-site ionic radii. The scatter of data-points especially for the *b* lattice parameter is due to a distinct dependence on the A-site

cationic radius. However, also the occupation of the A-sites plays and important role in controlling the size of the lattice parameter, with the samples with fully occupied A(1) and A(2)′ sites having the larger unit cell. The *c*-lattice parameter shows a strong correlation with the M-site cationic radius only, thus implying that *c* is quite insensitive to the average A-site cationic radius.

(3) The average M(1)-O bond length is larger in hagendorfite as compared to alluaudite. This can be explained by the presence of divalent cations (Fe^{2+}) with a larger average cationic M(2) size as compared to the smaller one in alluaudite *s.s.* with only ferric iron on M(2). This behaviour implies a distinct influence of the size of the M(2) site cations onto the average bond lengths at the M(1) site.

(4) The M(1) site in alluaudite shows a large angular distortion which, however, decreases when the cationic radius of the neighbouring M(2) sites approaches the size of the M(1) cation. The lowest angular distortion is observed for the protonated un-oxidized samples having the M(1) and the M(2) site occupied by the same kind of cations. Here, the negative correlation holds true between angular M(1) site distortion and size of the M(1) cation.

(5) In alluaudite *s.s.* from Buranga-pegmatite iron is in the trivalent state only. In contrast to claims in the literature there is no distribution for the quadrupole splitting of Fe^{3+}. Instead, the spectrum of alluaudite can satisfactorily be evaluated with a single symmetric Lorentzian-shaped doublet. However, as shown by Hatert *et al.* (2004), alluaudite also may show some minor amounts of ferrous iron.

Acknowledgement: GJ Redhammer's research was financed by the Austrian "Fonds zur Förderung der Wissenschaftlichen Forschung" (FWF) throughout grant R33-N10 which is gratefully acknowledged. The paper benefited from the thorough reviews of Frederic Hatert and Kim Tait, which also is acknowledged very much.

References

Antenucci, D., Miehe, G., Tarte, P., Schmal, W.W., Fransolet, A.-M. (1993): Combined X-ray Rietveld, infrared and Raman study of a new synthetic variety of alluaudite, $NaCdIn_2(PO_4)_3$. *Eur. J. Mineral.*, **5**, 207-213.

Antenucci, D., Fransolet, A.M., Miehe, G., Tarte, P. (1995): Synthèse et cristallochimie de $NaCdIn_2(PO_4)_3$, phosphate nouveau à structure alluaudite sans cation trivalent. *Eur. J. Mineral.*, **7**, 175-181.

Ben Smail, R. & Jouini, T. (2004): $AgNi_3(PO_4)(HPO_4)_2$: an alluaudite-like structure. *Acta Cryst.*, **C8**, i61-i62.

Brese, N.E. & O'Keeffe, M. (1991): Bond-valence parameters for solids. *Acta Cryst.*, **B47**, 192-197.

Chouaibi, N., Daidouh, A., Pico, C., Santrich, A., Veiga, M.L. (2001): Neutron diffraction, Mössbauer spectrum, and magnetic behavior of $Ag_2FeMn_2(PO_4)_3$ with alluaudite-like structure. *J. Solid State Chem.*, **159**, 46-50.

Corbin, D.R., Witney, J.F., Fultz, W.C., Stucky, G.D., Eddy, M.M., Cheetham, A.K. (1986): Synthesis of open-framework transition metal phosphates using organometallic precursors in acid media. Preparation and structural characterization of $Fe_5P_4O_{20}H_{10}$ and $NaFe_3P_3O_{12}$. *Inorg. Chem.*, **25**, 2279-2280.

Daidouh, A., Durio, C., Pico, C., Veiga, M.L., Chouaibi, N., Ouassini, A. (2002): Structure and electrical study of the alluaudites $(Ag_{1-x}Na_x)_2FeMn_2(PO_4)_3$ (x = 0, 0.5 and 1). *Solid State Sci.*, **4**, 541-548.

Dowtey, E. & Lindsley, D.H. (1973): Mössbauer spectra of synthetic hedenbergite-ferrosilite pyroxenes. *Am. Mineral.*, **58**, 850-868.

Durio, C., Daidough, A., Chouaibi, N., Pico, C., Veiga, M.L. (2002): Electrical behavior of new orthophosphates $Na_2M_3(PO_4)_3$ (M_3 = $GaMn_2$, $GaCd_2$, $InMn_2$ and FeMnCd) with alluaudite-like structure. *J. Solid State Chem.*, **168**, 208-216.

Farrugia, L.J. (1999): WinGX suite for small-molecule single-crystal crystallography. *J. Appl. Cryst.*, **32**, 837-838.

Fisher, D.J. (1955): Alluaudite. *Am. Mineral.*, **40**, 1100-1109.

Fransolet, A.-M., Antenucci, D., Fontan, F., Keller, P. (1994): New relevant data on the crystal chemistry, and on the genetical problem of alluaudites and wyllieites. *Abstracts of the 16th IMA general meeting, Pisa*, 125-126.

Fransolet, A.-M., Keller, P., Fontan, F. (1997): The alluaudite group minerals: Their crystallochemical flexibility and their modes of formation in the granite pegmatites. *Abstracts of the meeting "Phosphates: biogenic to exotic", London*.

Fransolet, A.-M., Hatert, F., Fontan, F. (2004): Petrographic evidence for primary hagendorfite in an unusual assemblage of phosphate minerals, Kibingo granitic pegmatite, Rwanda. *Can. Mineral.*, **42**, 697-704.

Gaines, R.V., Skinner, H.C.W., Foord, E.E. (1997): Dana's New Mineralogy. 8th Edition, 1872 pp, Wiley-Interscience.

Guesmi, A. & Driss, A. (2004): $AgCo_3PO_4(HPO_4)_2$. *Acta Cryst.*, **C8**, i16-i17.

Hatert, F. (2002): Cristallochimie et synthèse hydrothermale d'alluaudites dans le système Na-Mn-Fe-P-O: contribution au problème de la genèse de ces phosphates dans les pegmatites granitiques. Unpublished Ph. D. Thesis, University of Liège, 247 p.

— (2004): The crystal chemistry of lithium in the alluaudite structure: a study of the $(Na_{1-x}Lix)_{1.5}Mn_{1.5}Fe_{1.5}(PO_4)_3$ solid solution (x = 0 to 1). *Min. Petrol.*, **81**, 205-217.

Hatert, F., Keller, P., Lissner, F., Antenucci, D., Fransolet, A.M. (2000): First experimental evidence of alluaudite-like phosphates with high Li-content: the $(Na_{1-x}Lix)MnFe_2(PO_4)_3$ series (x = 0 to 1). *Eur. J. Mineral.*, **12**, 847-857.

Hatert, F., Antenucci, D., Fransolet, A.-M., Liegeois-Duyckaerts, M. (2002): The crystal chemistry of lithium in the alluaudite structure: a study of the $(Na_{1-x}Li_x)CdIn_2(PO_4)_3$ solid solution (x = 0 to 1). *J. Solid State Chem.*, **163**, 194-201.

Hatert, F., Hermann, R.P., Long, G.J., Fransolet, A.-M, Grandjean, F. (2003): An X-ray Rietveld, infrared, and Mössbauer spectral study of the $NaMn(Fe_{1-x}In_x)_2(PO_4)_3$ alluaudite-type solid solution. *Am. Mineral.*, **88**, 211-222.

Hatert, F., Long, G.J., Hautot, D., Fransolet, A.-M., Delwiche, J., Hubin-Franskin, M.J., Grandjean, F. (2004): A structural, magnetic, and Mössbauer spectral study of several Na-Mn-Fe-bearing alluaudites. *Phys. Chem. Minerals*, **31**, 487-506.

Hatert, F., Rebbouh, L., Hermann, R.P., Fransolet, A.-M., Long, G.J., Grandjean, F. (2005): Crystal chemistry of the hydrothermally synthesized $Na_2(Mn_{1-x}Fe^{2+}{}_x)_2Fe^{3+}(PO_4)_3$ alluaudite-type solid solution. *Am. Mineral.*, **90**, 653-662.

Hermann, R.P., Hatert, F., Fransolet, A.-M., Long, G., Grandjean, F. (2002): Mössbauer spectral evidence for next-nearest neighbor

interactions within the alluaudite structure of $Na_{1-x}Li_xMnFe_2(PO_4)_3$. *Sol. State Sci.*, **4**, 507-513.

Hidouri, M., Lajmi, B., Driss, A., Amra, M.B. (2004a): The alluaudite-like phosphate $Na_{1.79}Mg_{1.79}Fe_{1.21}(PO_4)_3$. *Acta Cryst.*, **C9**, i7-i9.

Hidouri, M., Lajmi, B., Wattiaux, A., Fournes, L., Darriet, J., Amara, M. (2004b): Characterization by X-ray diffraction, magnetic susceptibility and Mössbauer spectroscopy of a new alluaudite-like phosphate: $Na_4CaFe_4(PO_4)_6$. *J. Solid State Chem.*, **177**, 55-60.

Ingalls, R. (1964): Electric-field gradient tensor in ferrous compounds. *Phys. Rev.*, **133**, A787-A795.

Korzenski, M.B., Schimek, G.L., Kolis, J.W. (1998): Hydrothermal synthesis, structure and characterization of a mixed-valent iron (II/III) phosphate, NaFe3.67(PO4)3: a new variation of the alluaudite structure type. *J. Solid State Chem.*, **139**, 152-160.

Leroux, F., Mar, A., Payen, C., Guyomard, D., Verbaere, A., Piffard, Y. (1995a): Synthesis and structure of $NaMn_3(PO_4)(HPO_4)_2$, an unoxidized variant of the alluaudite structure type. *J. Solid State Chem.*, **115**, 240-246.

Leroux, F., Mar, A., Guyomard, D., Piffard, Y. (1995b): Cation substitution in the alluaudite structure type: Synthesis and structure of $AgMn_3(PO_4)(HPO_4)_2$. *J. Solid State Chem.*, **117**, 206-212.

Lii, K.H. & Shih, P.F. (1994): Hydrothermal synthesis and crystal structures of $NaCo_3(PO_4)(HPO_4)_2$ and $NaCo_3(AsO_4)(HAsO_4)_2$: synthetic modifications of the mineral alluaudite. *Inorg. Chem.*, **33**, 3028-3031.

Lii, K.H. & Ye, J. (1997): Hydrothermal synthesis and structures of $Na_3In_2(PO_4)_3$ and $Na_3In_2(AsO_4)_3$: synthetic modifications of the mineral alluaudite. *J. Solid State Chem.*, **131**, 131-137.

Moore, P.B. (1971): Crystal Chemistry of the alluaudite structure type: Contribution to the paragenesis of pegmatite giant crystals. *Am. Mineral.*, **56**, 1955-1975.

Moore, P.B. & Ito, J. (1979): Alluaudites, wyllieites, arrojadites: crystal chemistry and nomenclature. *Min. Mag.*, **43**, 227-235.

Mücke, A. (1981): The parageneses of the phosphate minerals of the Hagendorf pegmatite - A general view. *Chem. Erde*, **40**, 217-234.

Pennington, T. (1999): DIAMOND - Visual crystal structure information system. *J. Appl. Cryst.*, **32**, 1028 (1999).

Rancourt, D.G. & Ping, J.Y. (1991): Voigt-based methods for arbitrary-shape static hyperfine parameter distribution in Mössbauer spectroscopy. *Nucl. Instrum. Meth. Phys. Res.*, **B 58**, 85-97.

Rancourt, D.G., McDonald, A.M., Lalonde, A.E., Ping, J.Y. (1993): Mössbauer absorber thickness for accurate site populations in Fe-bearing minerals. *Am. Mineral.*, **78**, 1-7.

Redhammer, G.J. & Roth, G. (2002): Single-crystal structure refinements and crystal chemistry of synthetic trioctahedral micas $KM_3(Al^{3+}, Si^{4+})_4O_{10}(OH)_2$, where M = Ni^{2+}, Mg^{2+}, Co^{2+}, Fe^{2+}, or Al^{3+}. *Am. Mineral.*, **87**, 1464-1476.

—,— (2004): Structural variation and crystal chemistry of $LiMe^{3+}Si_2O_6$ clinopyroxenes Me^{3+} = Al, Ga, Cr, V, Fe, Sc and In. *Z. Kristallogr.*, **219**, 278-294.

Redhammer, G.J., Tippelt, G., Roth, G., Lottermoser, W., Amthauer, G. (2000): Structure and Mössbauer spectroscopy of barbosalite $Fe^{2+}Fe^{3+}{}_2(PO_4)_2(OH)_2$. *Phys. Chem. Minerals*, **27**, 419-429.

Redhammer, G.J., Roth, G., Tippelt, G., Bernroider, M., Lottermoser, W., Amthauer, G. (2004): The mixed-valent iron compound $Na_{0.1}Fe_7(PO_4)_6$: crystal structure and ^{57}Fe Mössbauer spectroscopy between 80 K and 295 K. *J. Sol. State Chem.*, **177**, 1607-1618.

Renner, B. & Lehmann, G. (1986): Correlation of angular and bond length distortion in TO_4 units in crystals. *Z. Kristallogr.*, **175**, 43-59.

Robinson, G., Gibbs, V., Ribbe, P.H., (1971): Quadratic elongation, a quantitative measure of distortion in coordination polyhedra. *Science*, **172**, 567-570.

Shannon, R.D. & Prewitt, C.T. (1969): Effective ionic radii in oxides and fluorides. *Acta Cryst.*, **B25**, 925-934.

Sheldrick, G.M. (1997): SHELXS-97 and SHELXS-97. Programs for crystal structure solution. University of Göttingen, Germany (1997).

Stoe & Cie (1996): X-SHAPE and X-RED: Programs for optimization of the crystal shape (w.r.t the merging R-value) and numerical absorption correction. Stoe & Cie (Darmstadt, Germany, 1996)

Strunz, H. (1954): Hagendorfit, ein neues Mineral der Varulith - Hühnerkobelit - Reihe. *N. Jahrb. Min. Monatsh.*, **1954**, 252-255.

Toraya, H. (1986): Distortion of octahedra and octahedral sheets in 1*M* micas and the relation to their stability. *Z. Kristallogr.*, **157**, 173-190.

Warner, T.E., Milius, W., Maier, J. (1993): Synthesis and structure of $Cu_{1.35}Fe_3(PO_4)_3$ and $Cu_2Mg_3(PO_4)_3$: new mixed valence compounds of the alluaudite structure type. *J. Solid State Chem.*, **106**, 301-309

Wilson, A.J.C. (1992): Ed. International Tables for Crystallography, Volume C, Kluwer Academic Publishers, Dordrecht, The Netherlands.

Received 17 October 2004
Modified version received 4 April 2005
Accepted 30 May 2005